Comparison of Hydrocracking Activities and Selectivities of Catalysts Prepared by Incipient Wetness and Supercritical Deposition

by

İbrahim Şahin

A Thesis Submitted to the
Graduate School of Sciences and Engineering
in Partial Fulfillment of the Requirements for
the Degree of

Master of Science
in
Chemical and Biological Engineering

Koc University

September 2014

Koc University

Graduate School of Sciences and Engineering

This is to certify that I have examined this copy of a master's thesis by

İbrahim ŞAHİN

and have found that it is complete and satisfactory in all respects,
and that any and all revisions required by the final
examining committee have been made.

Committee Members:

_____

Can Erkey, Ph. D. (Advisor)

_____

Yaman Arkun, Ph. D.

_____

Murat Sözer, Ph. D.

Date: _____

to my family...

ABSTRACT

Hydrocracking is the most profitable operation in the petroleum refinery due to its role of converting heavy petroleum cuts, such as gas oil and asphaltenes, to the more valuable products like diesel and heavy naphtha. The process involves the cracking of long chained hydrocarbons followed by hydrogenation of the cracked chains. Thus, the catalyst used in hydrocracking has both cracking and hydrogenation function which are generally supplied from an acidic support and loaded noble or earth metal. The balance between these two functions makes the hydrocracking process very flexible for the production of wide range of products from variety of feed stocks. In this study, the aim was to compare hydrocracking activities and selectivities of catalysts prepared by two different methods as incipient wetness and supercritical deposition. For this purpose, three commercial were selected as reference materials. N-decane was chosen as a model feed in order to have better understanding of catalysts by tracking the product distributions using GC-MS for preliminary studies. Supports were prepared with different amounts silica-alumina, USY zeolite and Ludox binder. The characterization of synthesized materials was performed by XRF, N_2 physisorption and TPD. Then, three different types of catalysts, commercial, prepared by impregnation and by supercritical deposition (SCD) methods, were tested for n-decane reactions in a laboratory scale plug flow trickle bed reactor which was developed during this study. Furthermore, heavy vacuum gas oil was replaced with n-decane and catalyst performance tests were repeated for this feed. The product analyses were done with ASTM standard distillation and GC Simdist analaysis, which was in agreement with the former. Finally, kinetic modelling of gas oil cracking was done using discrete lumping method in order to compare kinetic parameters of the catalysts. Results showed catalysts prepared with impregnation and supercritical deposition methods had comparable activities relative to the commercial catalysts for both n-decane and gas oil hydrocracking.

Moreover, the catalysts prepared by SCD method had a superior activity and slightly higher middle distillate selectivity than the other catalysts. This finding was also supported by the results of the modeling studies.

ÖZET

Gaz yağı ve asfalten gibi ağır petrol fraksiyonlarını dizel ve nafta benzeri hafif ve değerli ürünlere dönüştürdüğünden dolayı, hidrokraker ünitesi petrol rafinerisinin en karlı ünitesidir. Bu işlem uzun zincirli hidrokarbonların kırılması ve bunu takiben kırılan zincirlerin hidrojenle doyurulmasını içermektedir. Bu sebeple, hidrokraker katalizörü hem kırma hem hidrojenleme fonksiyonlarına sahiptir, bunlar genellikle asidik destek malzemesiyle ve buna yüklenmiş soy ya da soy olmayan metallerle sağlanır. İki fonksiyon arasındaki denge, çeşitli beslemenlerden geniş yelpazede ürün eldesi sağlarak hikdrokraker işlemini esnek hale getirir. Bu çalışmadaki amaç, gözenek hacminde çözelti emdirme ve süperkritik depozisyon yöntemleriyle hazırlanmış katalizörlerinin aktivite ve seçiçiliğini karşılaştırmaktır. Bu amaçla, üç adet ticari katalizör referans malzemesi olarak kullanılmıştır. Öncül çalışmalarda, GC-MS kullarak ürün dağılımını takip ederek katalizörleri daha iyi incelemek amacıyla n-dekan model bir besleme olarak seçilmiştir. Destek malzemeleri farklı miktarlarda silica-alümina, USY zeolite ve Ludox bağlayıcı malzemesi kullanılarak hazırlanmıştır. Sentezlenen malzemelerin karakterizasyonları XRF, azor fizisorpsiyonu ve TPD kullarak yapılmıştır. Üç farklı katalizör, ticari, gözenek hacminde sıvı emdirme yöntemiyle hazırlanmış ve süperkritik depozisyon yöntemiyle hazırlanmış olmak üzere, bu çalışma boyunca geliştirilen laboratuvar ölçekli tapa akışlı damlacıklı reaktörde test edilmiştir. Daha sonra dekan yerine ağır gaz yağı kullanarak, katalizör testleri tekrarlanmıştır. Ürün analizleri birbirine uyumlu olan ASTM standard distilasyon ve GC simüle distilasyon yöntemleriyle yapılmıştır. Son olarak farklı katalizlerin kinetik parametrelerini karşılaştırma amacıyla, ağır gaz yağı reaksiyonu modellemesi ayrık gruplama yöntemiyle yapılmıştır. Sonuçlar, sentezlenen katalizörlerin ticari katalizör ile karşılaştırılabilir aksitivitesi olduğunu göstermiştir. Ayrıca, süperkritik depozisyon yöntemiyle sentezlenen katalizör üstün bir aktiviteye ve biraz daha iyi orta

distilat seçiciliğine sahip olduğu görülmüştür. Bu bulgular modelleme sonuçları ile desteklenmiştir.

ACKNOWLEDGEMENTS

First, I would like to thank you my advisor Prof. Dr. Can Erkey to give me the opportunity to perform research activities in his group, allow me to pursue M.Sc. degree in Koç University and more importantly his guidance and vision.

I acknowledge the financial support of the Tüpraş and its supplying me the necessary equipment of materials during tthe project. I would also like to gratefully and sincerely thank to my thesis committee members Prof. Dr. Yaman Arkun and Assoc. Prof. Dr. Murat Sözer for their careful reading and comments for my thesis and its presentation.

I also send my regards to Ihsan Ozan Yıldırım for sharing his time and support. I should also thank Selin İsmet for her sincere support and presence. I thank Metin Karayılan for his supportive and presence from the start of my life in Koç University. I would like to thank you my group member Deniz Şanlı, Selmi Erim Bozbağ, Yaprak Özbakır, Gamze Eriş, Göktuğ Gönen. I also thank Ramazan Oğuz Canıaz for his ideas and guidance through my university life.

I would like to especially thank my family for their love, patience and continuous support they have given me throughout my entire life. Finally, I thank my unborn nephew Ufuk Sırrı Erinç for the excitement and joy brought by his presence.

TABLE OF CONTENTS

LIST OF TABLES

LIST OF FIGURES

NOMENCLATURE

A = frequency factor, volume of feed/(volume of catalyst h)

B, *C* = product distribution parameters, (-)

Ci = mass fraction of pseudocomponent *i* in the mixture, (-)

Di = constants for relative rate expression (*i*)

E = activation energy, kcal/kmol

ki, *kj* = overall first-order reaction rate constant for the cracking of pseudocomponent, kg of reactant/(kg of catalyst h)

Ki = relative reaction rate function

*M*t = mass flow rate of feed, kg/h

N = number of pseudocomponents

R = ideal gas constant, 2.0 cal/(mol K)

T = operating reactor temperature, K

*T*b*j* = boiling point of pseudocomponent *j*, °C

W = weight of the catalyst bed, kg

yij = normalized boiling point of pseudocomponent *i* to pseudocomponent *j*, (-)

V*i* = volume of the petroleum cut i

Subscripts/*Superscripts*

i, *j*(-)

Chapter 1

INTRODUCTION

Hydrocracking is one of the most important processes in petroleum refinery due to conversion of heavy fractions in to lighter and valuable products. The process is also very flexible because of the wide range of feedstocks and desired products. The hydrocracking capacity of Asia-Pacific, Middle East and Europe countries has been increasing over past years and it is estimated that they will continue to increase for the near future [1]. Thus, researches for improvements in hydrocracking process by means of activity and desired product will be play a crucial role in petroleum industry. These improvements were generally realized by developing effective catalysts.

Hydrocracking involves the cracking of long chained hydrocarbons followed by hydrogenation of the cracked chains. Thus, the catalyst used in hydrocracking has both cracking and hydrogenation function which are generally supplied from an acidic support and loaded noble or earth metal. Silica alumina and zeolites were extensively used to provide cracking functions whereas hydrogenation function was supplied from platinum, palladium sulfide and promoted group VI sulfides, nickel molybdenum or nickel tungsten[2, 3]. The balance between cracking and hydrogenation function is generally set in agreement with the process needs. Tuning of the properties of the support is very important for having desired product selectivity. Zeolite supports are more active than the amorphous supports due to high number of acid sites and superior acid strength [1]. However, silica alumina supported catalysts are better for obtaining middle distillates whereas the use of zeolite supports will lead to the production of naphtha and gasoline. On the other hand, appropriate mixtures of the two can also be used for maximizing both middle distillate selectivity and activity. Loading of hydrogenation metals is also very

important to prevent coke formation during the process. Hydrogenation of the alkenes should take place swiftly before the start of any polymerization or condensation reactions which will lead to the formation of coke precursors [4]. A good dispersion of metals and a proper metal-acid balance should also be obtained to have an effective catalyst.

In this project, the main goal is to develop an effective supported Ni-W catalyst for hydrocracking of heavy vacuum gas oil. For this purpose, we compared hydrocracking activities and selectivities of catalysts prepared by two different methods as incipient wetness and supercritical deposition.

In Chapter 2, necessary literature review on hydrocracking process and catalysis was provided. Catalysts preparation methods along with previously used supports and metals were explained. Moreover, a brief review on kinetic modeling of hydrocracking of heavy vacuum gas oil was included.

Chapter 3 provided experimental methods used in this study. Starting with the used materials, hydrocracking reaction system, catalysts characterization techniques and product analysis were explained. Experimental procedures for the support and catalysts preparation and performance tests were supplied. Finally, description of the constructed model and the parameter estimation technique was presented.

Results of the catalysts preparation, characterization and the performance tests were given in Chapter 4. Comparison the catalysts in terms of activity and diesel selectivity were done using these results. The kinetic parameters estimated from the model were also compared in this section.

Chapter 5 finalized the thesis by stating the main outcomes arrived in this project.

Chapter 2

LITERATURE REVIEW

2.1 Hydrocracking Process

A simple definition of hydrocracking is the decomposition of hydrocarbons on the acid sites of the catalyst's support, followed by hydrogenation of the cracking products on the metallic sites [4]. The main role of this process in modern refineries is the conversion of heavy vacuum gas oil to middle distillates such as diesel and kerosene. Figure 2.1 shows that hydrocracking capacity of refineries has been increasing through past decades.

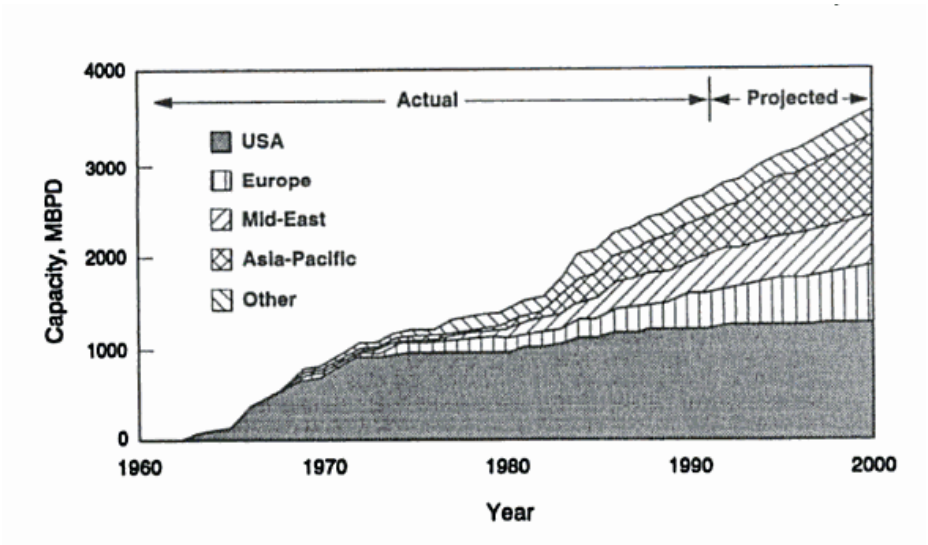

Figure 2.1 Actual and projected worldwide hydrocracking capacity in year 1996, adopted from [2].

U.S catalytic hydrocracking capacity has been increased from 1.6 million barrel per stream day to 2.2 million within 10 years [5]. Thus, the process will also play a key role in refining industry in near future.

In order to better understand the role of hydrocracking, it is better to investigate the units in a modern refinery. Figure 2.2 shows that feed to the hydrocracker is delivered from the vacuum distillation. This feed is called heavy vacuum gas oil and it is consisted of several hydrocarbons having carbon numbers between 25-40 [1]. On the other hand jet fuel and kerosene, which are the main products of a hydrocracker, have carbon numbers between 10-20 [1]. So, an appreciable amount of cracking of long hydrocarbons is essential. In early refineries, cracking function is generally supplied from thermal cracking and fluid catalytic cracking (FCC) units. The main disadvantage of pyrolysis is that certain amounts of polymerized heavier products (i.e. coke) is always formed along with the gasoline and petroleum gas [6]. Similarly, the absence of hydrogen in catalytic cracking units leads to formation of coke on catalysts surfaces, which will eventually decrease the activity and thus the product yield of the unit. On the other hand, preventing the formation of coke via hydrocracking will eventually boost the yield of the desired product. Another problem with the catalytic cracking is that over cracking of the gas oils decrease the yield of middle distillates and increase the formation of light naphtha and gases. Besides, the presence of isomerized alkanes, which boost the quality of the final fuel by increasing its octane number, cannot be obtained at high cracking yields. In a modern refinery catalytic cracking and hydrocracking work in harmony so that the catalytic cracker takes the more easily cracked paraffinic atmospheric and vacuum gas oils as charge stocks, while the hydrocracker uses more aromatic cycle oils and coker distillates as feed [7]. Thus, gasoline is produced as the main product of FCC units whereas diesel and kerosene are produced by hydrocracker units as in the figure below.

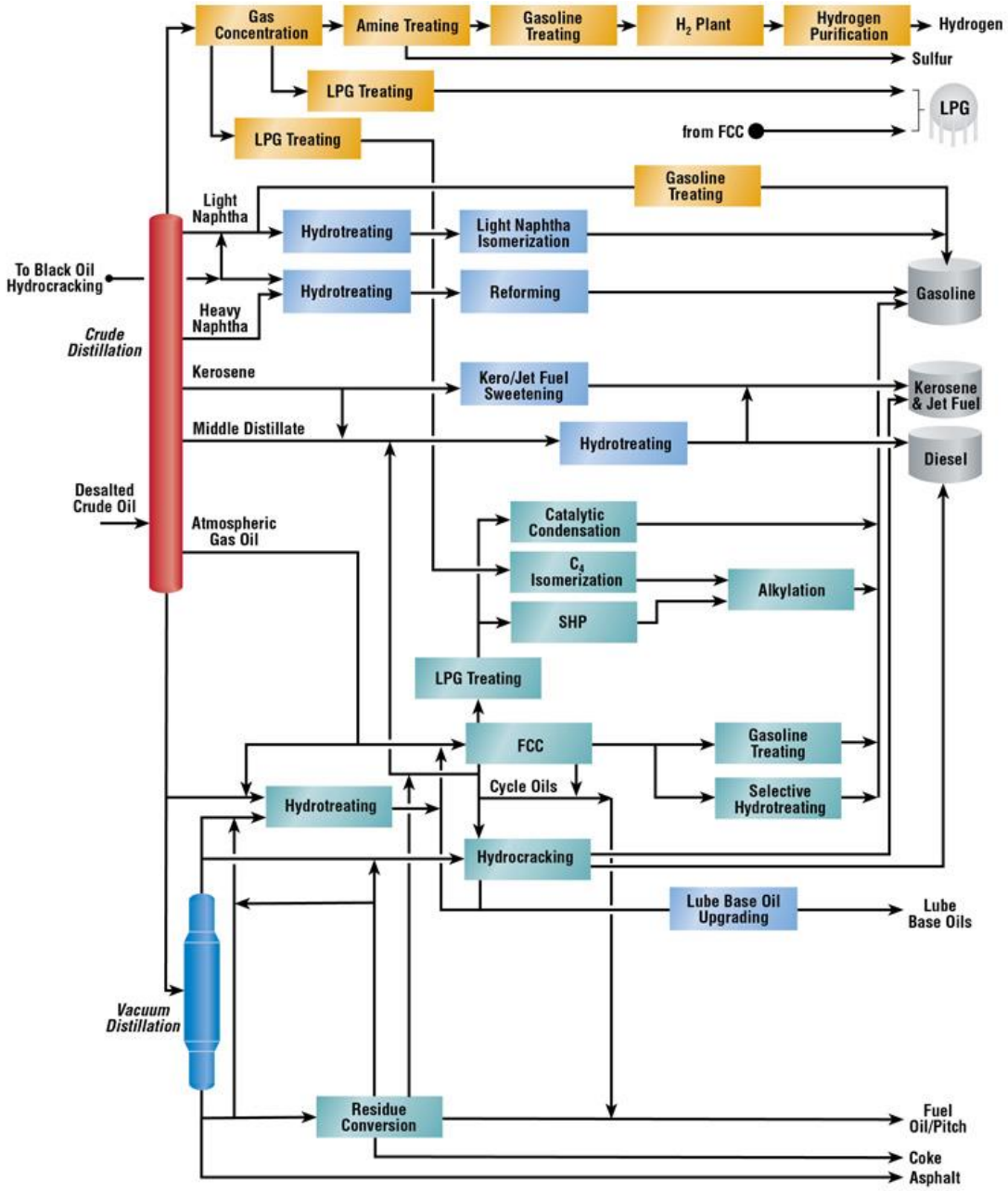

Figure 2.2 Simplified Refining Flow Scheme, retrieved from [8]

Hydrocracking units operate at high temperatures and pressures and involve the use of hydrogen, see figure below. For this reason, it is a very expensive operation and any improvements in the process conditions will be very profitable.

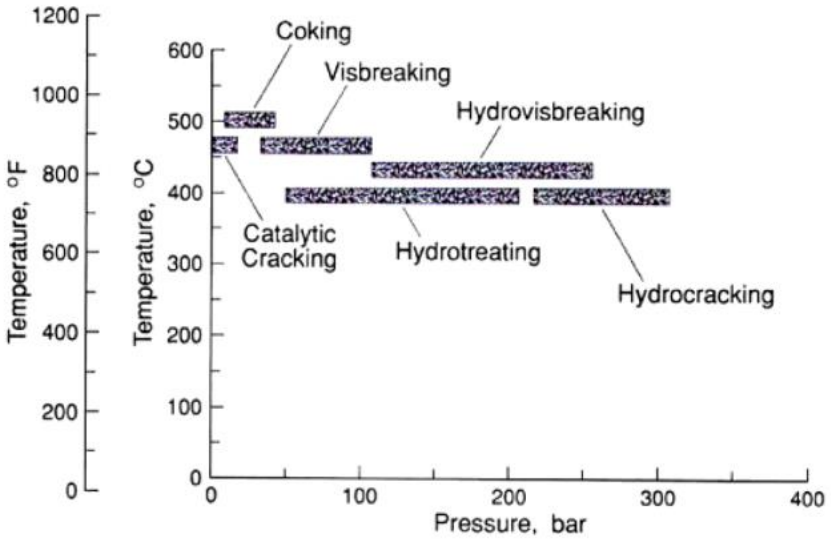

Figure 2.3 Temperature and pressure parameters of various refinery processes, adopted from [2].

In practice, several reactions take place in a hydrocracker. They can be summarized as hydrodesulfurization, hydrodenitrification, olefin hydrogenation, saturation of aromatic and hydrocracking and hydroisomerization of large molecules [3, 4]. First four reactions take place in metallic site of the catalysts whereas supports are responsible for cracking and isomerization reactions. For this reason, it is a very complicated unit and there is still room for technological advancement. Properties of the feed and type of the desired products generally govern the implantation of the process. Commonly, hydrocrackers were at two stage operations. Removal and sulfur and nitrogen containing compounds is performed at the first stage. The acidity of the corresponding catalyst support is relatively low. The

second stage is where hydrocracking reactions takes place. So, the first stage can be recognized as a purification step. The acidity of the second stage is relatively high. Noble metals such as Pt and Pa can be used at this stage because of the absence of sulfur containing organic compounds (Noble metals are prone to poisoning by sulfur and nitrogen).

2.2 Hydrocracking of Alkanes

In order to understand the role of catalysts and the chemistry of the reactions, it is beneficial to investigate the hydrocracking alkanes. Several studies investigated hydrocracking reaction of the decane, octane and hexadecane in order to better understand reaction mechanism and catalytic interactions [9-18]. The studies conclude that following steps governs mechanism of n-alkane hydrocracking;

- Dehydrogenation on metallic sites
- The adsorption of alkenes on acid sites with formation of carbenium ions
- Isomerization and cracking on the acid sites
- Hydrogenation of the alkenes resulting from isomerization and cracking on the metallic sites

Weitkamp summarized the reactions undergo during this mechanism as in the figure below[9].

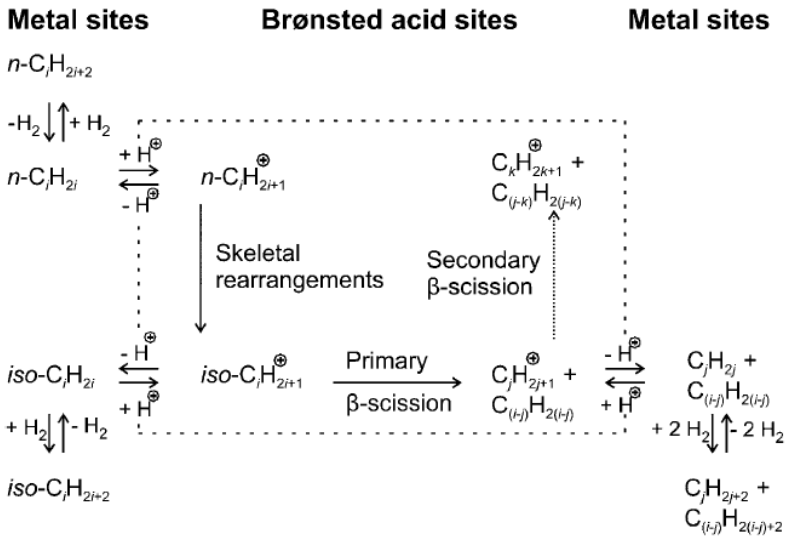

Figure 2.4 Classical mechanism of isomerization and hydrocracking of an n-alkane on a bifunctional catalysts [9].

Rezgui et. al studied the effect of acidity and metal content on the activity and selectivity for n-decane reactions using Ni-W on silica-alumina catalysts [10]. He found that cracking rate increased with the increasing acid strength at the expense of hydroisomerization. He also found that amount of metal content strongly affected the catalytic performance. The activity of the catalysts improved with the amount of metal contents whereas there was a limitation for the improvement in the case of isomerization. Roussel et.al found the behavior of the Ni-W catalysts in the presence of nitrogen containing compounds was different from the findings above due to the poisoning the acid sites [18]. Steijns et. al studied product distributions of n-decane and n-dodecane reaction on Pt/USY catalysts [16]. They found that isomerization selectivity of paraffins is unique

function selectivity. Besides, the chain length affected the distributions of the branched alkanes in cracking products by increasing the fraction of branched alkanes.

2.3 Hydrocracking Catalysts

Hydrocracking catalysts are generally supported catalysts due to the necessity to have a dual function. Silica alumina and zeolites were extensively used to provide cracking functions whereas hydrogenation function was supplied from platinum, palladium sulfide and promoted group VI sulfides, nickel molybdenum or nickel tungsten[2, 3]. Compositional and structural properties of the catalysts are generally tuned in accordance with the feed and desired products. Table 2.1 shows the properties of the commonly used support and metals. According to this table, zeolites are better for obtaining lighter products like naphtha and gasoline whereas alumina and silica alumina perform well for middle distillate selective cracking. The choice of metal is depends on the presence of heteroatoms in the feed. Pt and Pa are more prone to poisoning by sulfur; Ni/Mo is, however, is no limitation and Ni/W lies between these two [4].

Table 2.1 Bifunctional hydrocracking catalysis, adopted from [19].

	Hydrogenation function	Acidic function (support)	
Increasing	↓ Ni/Mo	Al_2O_3	↓ Increasing
Hydrogenation Power	Ni/W	Al_2O_3/halogen	Acidity
	Pt/Pd	SiO_2/Al_2O_3	
		Zeolites	
	(low-S conditions)		

2.3.1 Hydrocracking Catalyst Supports

Silica-alumina and several zeolite types, such as USY, HSZ and beta, have been used extensively in hydrocracking catalysts. In principle, zeolites, which have higher number of strong acid sites, are more active than amorphous Si/Al [1]. Both have similar chemistry at the molecular level. Zeolites consist primarily of silicon, aluminum, and oxygen and host an assortment of other elements. In addition, zeolites are highly porous crystals veined with submicroscopic channels [20]. Like the Si/Al catalysts, zeolites also consist of a framework of tetrahedral usually with a silicon atom or an aluminum atom at the center [20]. However, during hydrocracking zeolites were found to be more stable than amorphous Si/Al.

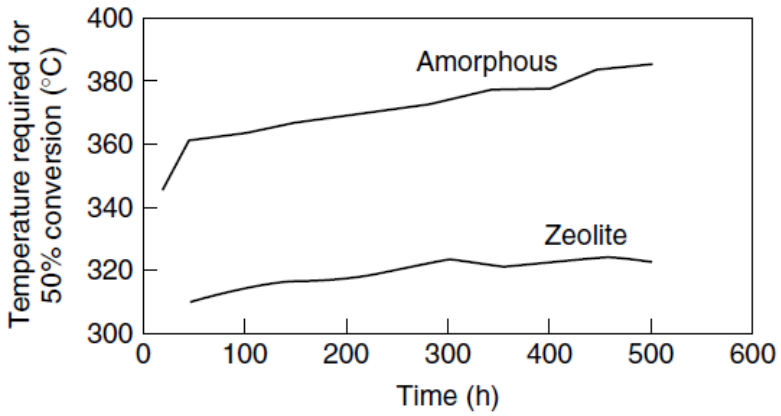

Figure 2.5 Deactivation rates of amorphous and zeolite catalysts in the hydrocracking of a hydrotreated vacuum gas oil, adopted from [19].

Figure 2.5 indicates even in the absence of heteroatoms, zeolite supports are more stable due to the cracking of coke precursors forming at the surface to supports. Besides, pore structure of the supports was shown to affect the selectivity of the catalyst. The introduction of mesoporosity to the support was found to enhance the middle distillate selectivity whereas micropores caused an increase in gas production [21]. Y zeolite, which

has accessible pore structure, was the best one of the best performing supports. The problem with Y-zeolites is that high boiling point molecules cannot access it, so, Si/Al can be added to create megaspores and overcome diffusion limitation. Moreover, mesoporosity obtained by ultrastabilization of zeolite-Y materials has been shown to reduce mass-transport limitations during hydrocracking and thus suppress secondary cracking [19]. Because of the good acidic and geometrical properties of Y-zeolites, ultrastabilized versions (USY) of it, great number of research efforts have been dedicated the usage of them along with Si/Al in hydrocracking catalysts [22-28].

2.3.2 Hydrogenation Metals

As discussed in previous sections, hydrogenation metals used in hydrocracking are selected in accordance with the feed properties. Pa and Pt have superior hydrogenation function but they are prone to poisoning. Besides, a good dispersion should be achieved for a good hydrogenation activity. For this reason, Ni is used along with W and Mo. The reason W and Mo addition is to increase the stability of the catalyst along with its poisoning resistance. Moreover, studies show that addition W, up 23-25 % by weight, boosts the acidity and activity of the catalyst [24, 29]. The efficiency of the catalyst is not only dependent on the proportions of metals but also on their appropriate dispersion [4]. A proper metallic site should have sufficient hydrodesulfurization, hydrodenitrification and olefin hydrogenation activities along with a dehydrogenation capability in order to start the mechanism in Figure 2.4. Metal and acid should be well-balanced in order to achieve the desired product yield.

2.3.3 Catalysts Preparation Methods

Preparation of hydrocracking catalysts is most commonly performed by impregnation methods. In most cases, the support itself prepared by extrusion of zeolite and Si/Al powders. Below figure show the summary of the typical preparation procedure.

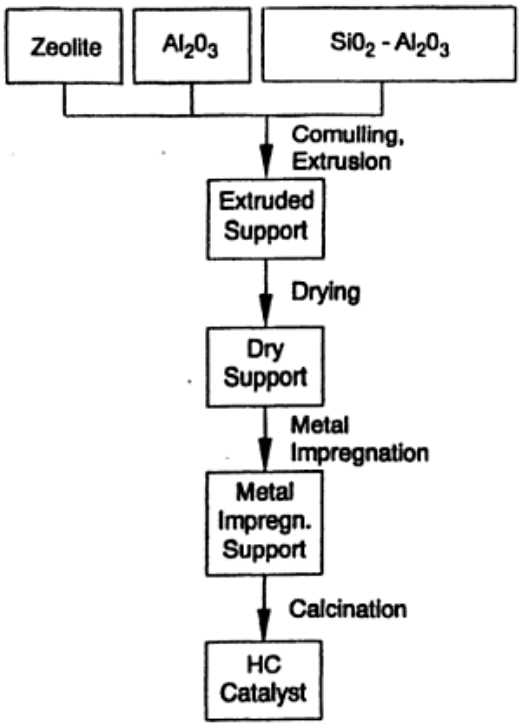

Figure 2.6 Flow diagram of a typical hydrocracking catalyst preparation, adopted from [1].

Impregnation method follows the addition of hydrogenation metal precursors to solution and diffusion of this solution to the pore system of the support by capillary forces. If the volume of metal precursor solution was equal to the pore volume of the support, the method is called incipient wetness. After the solution is impregnated, catalyst is dried and calcined to bring it to its final form. Although the amount of the metal content can be controlled easily in this method, the metal dispersion is in question. The degree of dispersion in the catalysts pellet is governed by the nature of the support surface, type of

the metal content, strength of interaction and chemical reactions that occur during drying [1].

Ion exchange is also one of the common methods when preparing catalysts with zeolite supports, due to ion exchange capacity of the zeolites. Noble metals can be loaded to the zeolite support in a w1ell dispersed manner. Non noble metals such as nickel and cobalt can also ion exchanged, however, Mo and W are not proper to use in this method because of their anionic form [1].

Supercritical deposition (SCD), which combines some characteristics of both vapor- and liquid-phase-based deposition techniques, has been attracting as an alternative technique for the preparation of novel nanostructured composites such as catalysts. In this approach, a metallic precursor is dissolved in a supercritical fluid followed by adsorption of it on the porous substrate. Subsequently, the adsorbed precursor is converted to its metal form by several techniques[30]. Supercritical CO_2 ($scCO_2$) is the most commonly used supercritical fluid due to low critical temperature, non-toxicity, non-flammability and being inexpensive. The liquid-like density of $scCO_2$ is several orders of magnitude higher than that of any gas, thus, it can dissolve larger concentrations of metal precursors. Additionally, the gas-like diffusivity and viscosity of $scCO_2$ are more favorable for rapid diffusion and permeation of solutes into porous substrates. The relatively low surface tension of $scCO_2$ provides better penetration and wetting of pores compared to conventional liquid solvents. It was recently shown that bimetallic Pt-Cu catalysts with controlled metal loading can be prepared on carbon aerogels using simultaneous SCD via tuning the thermodynamics of binary physical adsorption of metal precursors on supports [31]. Thus, this method can be a good candidate for supported bimetallic system which is generally the case in hydrocracking catalysts.

2.3.3.1 Recent Studies of Hydrocracking Catalyst Preparation

Recently, Yan et al. investigated the effect of impregnation methods by preparing three different catalysts; first pre-impregnating Ni-W to Y zeolite and mixing with Ni-W/zeolite to silica alumina, second pre-impregnating Ni-W to silica alumina and mixing with Y zeolite, finally impregnated to zeolite-silica alumina at once [32]. Results show that first catalysts had a strong hydrogenation performance and low acidity, which increase the diesel selectivity and inhibit the secondary cracking. Second catalysts had low hydrogenation capability and high acidity coordination which oppositely inhibit the increasing of catalytic activity and decrease the diesel selectivity. Ni-W uniform impregnated catalyst showed a better balance of hydrogenation ability and cracking ability of catalyst.

The study of Francis et al. used a similar approach by impregnating the Ni metal first on the USY zeolite then preparing composite catalysts NiMo/[γ-Al2O3 + (Ni)/USY] using the prepared Ni-USY zeolites [33]. It is claimed that enhanced conversion and middle distillate selectivity was obtained by this method due to an increased proximity between the hydrogenation/dehydrogenation function and the acid sites.

A different method based on loading of metals through metal vapors was utilized by Akhmedov et al.[34]. Zr-containing ZSM supported catalysts were loaded with Ni and Re. The catalysts were tested with octane cracking reaction. Ni containing bimetallic catalysts was found to have very high activity and C-C bond cleavage selectivity comparing to the support itself and other synthesized catalysts.

A novel method was recently proposed by Liu et al. for preparation of Ni-MoLa/γ-alumina catalyst [35]. In this study, powder metallurgy, which is a conventional dry powder processing technique, was used to prepare the catalysts and then, synthesized material was compared with the catalyst prepared by impregnation method. Comparisons showed that NiMoLa/γ-alumina catalysts from the new method led to a higher activity,

concluding that powder metallurgy could be a promising method in the preparation of hydrocracking catalysts.

Recent nanotechnology advancements were also used in hydrocracking catalysts. WS_2 catalysts as nanosheet structured particles were prepared and test in vacuum residue upgrading by Hur et al.[36]. Synthesized one layer WS_2 catalyst showed good commercial fuel production yield and metal removal activity due to the small particle size. Moreover, Alkhaldi et al. synthesized ultra-dispersed nickel nanocatalysts for hydrocracking of heavy oil [37].

2.4 Kinetic Modeling of Hydrocracking of Heavy Petroleum Fractions

Three methods have been used to model hydrocracking of heavy fractions. These are models based on lumping technique, models based on continuous mixtures, and structure oriented lumping and single event models. Lump models have been used for several years for kinetic modeling of complex reactions. Today, some commercial catalytic process design is still being performed with this type of approach. In such models, the feedstock is divided into several lumps, based on the boiling-point range. A simplified reaction network between these lumps is set up, then, the rate coefficients for the global conversion of lumps are estimated by matching with experimental data. For this reason, lumping methods fail to capture the chemistry of hydrocracking and they generally use simple models in which kinetic parameters strictly depends on feed properties [38, 39]. Second approach is based on continuum lumping in which the reaction mixture is considered to be a continuous mixture, with respect to the feed properties (boiling point and molecular weight). Continues mixture approach is also unable to capture the fundamental chemistry of the process [39, 40]. Elementary steps of cation chemistry, which consists of a limited number of types of steps involving series of homologous species are used in the single even concept [40]. Transition state theory and statistical thermodynamics was used

to reduce the number of rate coefficients to be determined from experimental information [39]. With this approach, parameter values are not dependent on feed properties, however, even though the number of parameters can be diminished, detailed and sufficient experimental data are necessary. Due to the complexity of the real feedstocks and necessity of heavy experimental work for detailed models, discrete lumping is still the most common method in kinetic modeling of heavy fractions.

Chapter 3

EXPERIMENTAL STUDIES AND KINETIC MODELING OF HEAVY VACUUM GAS OIL

3.1 Materials

Nickel nitrate hexahydrate [$Ni(NO_3)_2 \cdot 6H_2O$] (99.999 %; molecular weight = 290.79 g/mol, melting point = 56 °C), ammonium metatungstate hydrate [$(NH_4)_6H_2W_{12}O_{40} \cdot H_2O$] (99.99 %; molecular weight = 2974.3 g/mol, melting point = 100 °C), tungsten hexacarbonyl ($W(CO)_6$) (99.9 %; molecular weight = 351.91 g/mol, melting point = 150 °C), nickel(II) acetylacetonate ($Ni(acac)_2$) (95 %; molecular weight = 256.9 g/mol; melting point = 230°C) and Ludox HS-40 binder (40 wt. % SiO_2 suspension in H_2O) were purchased from Sigma-Aldrich. Amorphous silica-alumina (Al_2O_3 25 wt. %) with a surface area of 400 m^2/g was purchased from Saint-Gobain NorPro. USY zeolite powder in its H+ form was purchased from Tosoh Corporation (SiO_2/Al_2O_3 (mol/mol) = 6). Three different commercial catalysts were supplied from TÜPRAŞ. Water was distilled and deionized. Carbon dioxide (99.998 %), helium, oxygen and hydrogen were purchased from Messer Aligaz. A mixture of 10.5 % NH_3 in He was supplied by Elite Gaz.

N-decane [$C_{10}H_{22}$] (99 %; molecular weight=142.28), which used as model feed for preliminary studies, was purchased from Merck-Schuchardt OHG. HVGO feedstock was obtained from TÜPRAŞ. It was solid at room temperature and had a dark brown color with 2.46 wt% sulfur and 753 ppm nitrogen content.

3.2 General Equipment

All preparation, characterization and activity studies were carried out in Koç University while product analysis HVGO tests were performed by TÜPRAŞ using atmospheric and reduced pressure distillation and simulated distillation following corresponding ASTM standards.

3.2.1 Hydrocracking Reactor System

Activity tests of catalysts were performed using a custom made laboratory scale tubular plug flow reactor manufactured by Parr Instrument Company. Figure 3-1 shows a simplified flow diagram of the reactor system.

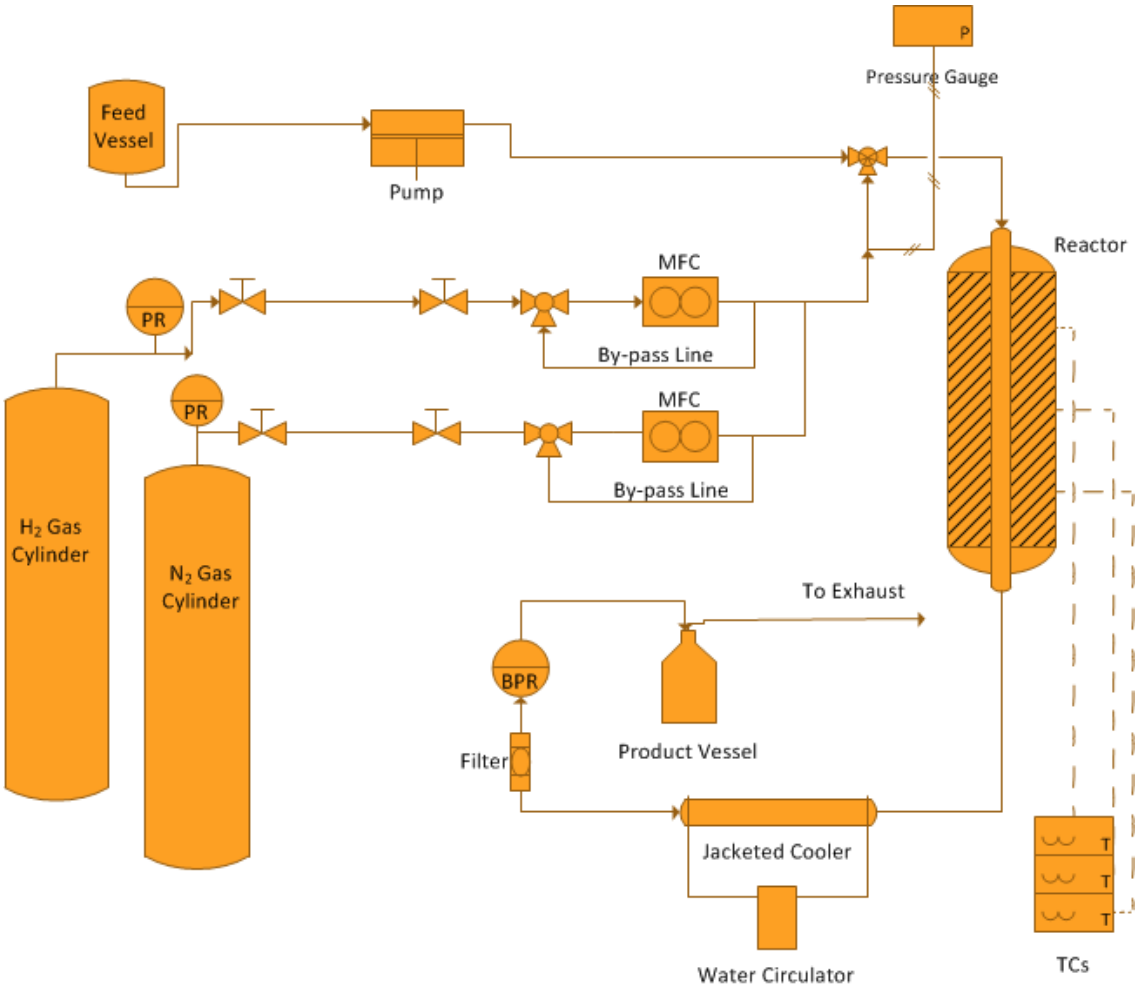

Figure 3-1 Simplified flow diagram of rector system**.**

A 1L feed tank having a relief valve and a heating mantle was connected to a HPLC pump with 1/8 inch tubing line. This line from vessel to pump could be heated using a heating tape in order to avoid blockage due to solidification of HVGO. Series III HPLC pump manufactured by Scientific Systems was used to deliver the feed to the reactor module. Flow rate could be set between 0.001- 5.00 ml/min whereas pressure range was 0-6000 psi. The head of the pump was heated using two heating rods. Reverse flow check

valves were placed before and after the pump for safety purposes. There is a pre-heater just before the entrance of the reactor for both avoiding blockage and make the temperature of the liquid feed reach the corresponding operating point. Reactor with catalyst volume of 40 cc was made of Alloy C-276, had a 0.37" ID, was rated for use to 3000 psi at 550 ºC, and is heated with a 24-inch long, three-zone, split-tube furnace (230 VAC) controlled with the use of thermocouples located in the outer wall of each 8"-long zone. Module also had INC safety rupture disc, SS pressure gage, and SS pressure transducer on the inlet manifold, as well as a movable thermocouple in a centerline thermowell (1/8"OD). A cooler made of C-276 alloy was placed between the reactor outlet and the back pressure regulator (BPR), which was used to adjust the operating pressure. Circulating cold water was used as coolant in this heat exchanger. A separator vessel with 300 ml capacity was present after the BPR to collect the liquid products. Hydrogen and nitrogen (being an inert gas) were fed from high pressure gas cylinders using mass flow controllers (MFC) manufactured by Brooks®. MFC's were calibrated for 2-100 sccm H_2 and N_2 at inlet pressure of 1800 psi and outlet pressure of 1500 psi. The maximum operating pressure of the MFC's was 4500 psi. Seven Parr Model 4838 temperature controllers were utilized to control the temperature of three heated zones on liquid feed system, three heated zones on the reactor, and one on the gas-liquid separator vessel. A Parr Model 0254 controller was used to set or display the two gas flow rates. The liquid flow rate was set on the face plate of the pump. Additional outside heaters were used to keep liquid flow when HVGO was used as feedstock. The actual picture of the reactor system can be seen in Figure 3-2**Error! Reference source not found.**.

Figure 3-2 Parr custom made reactor system used in catalysts testing**.**

3.2.2 Catalysts Characterization

Material characterization of all synthesized supports and catalysts were conducted using X-ray fluorescence (XRF) spectroscopy, N_2 physisorption and temperature programmed desorption (TPD) of NH_3. XRF was used to determine the chemical composition of materials by measuring the amounts of Si, Al, Ni and W. Surface area, pore size and pore volume were determined by using N_2 physisorption. TPD of NH_3 experiments were performed to measure the acidity of materials by means of mmol NH_3 adsorbed per gram of sample.

3.2.2.1 X-ray Fluorescence Spectroscopy

XRF is a non-destructive method which is used for measuring the elemental composition. When a sample is bombarded by x-ray, the atom may absorb and transfer this energy to the innermost shells. Ionization of inner shell, which means removal of an electron, causes the upper shell electron to fill the hole generated by this removal. The energy difference between two levels is emitted as x-ray fluorescence. Since every element has its unique energy levels between its shells, released fluorescence is characteristic to the corresponding element.[41] Figure 3-3 shows the schematic representation of the process.

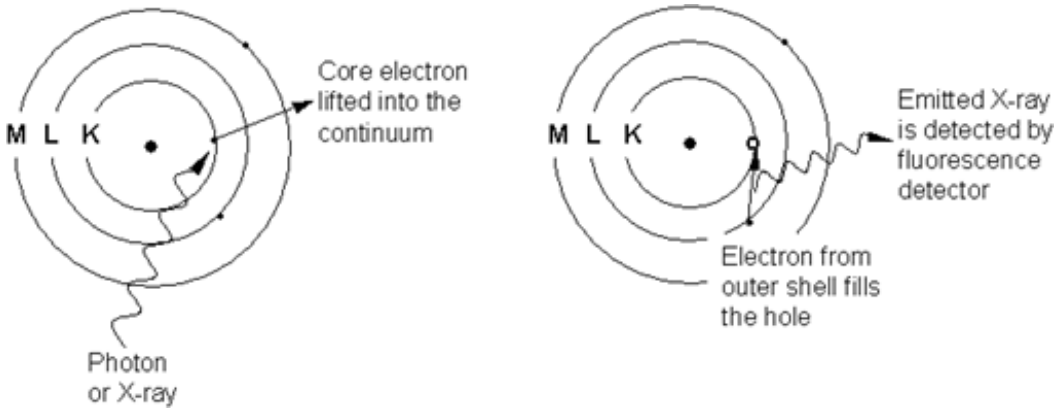

Figure 3-3 Representation of XRF analysis principle (*Retrieved from http://www.elementalanalysis.com/assets/12/xrf01.gif).*

Weight percentages Ni,W,Si and Al in the samples were determined using Bruker S8 Tiger X-ray Fluorescence (XRF) spectrometer which used Rh as the source of radiation. Powdered samples were placed on a 2.5 μm thick mylar sheet which was fixed in a sample cell. Measurement time was approximately 14 minutes. Figure 3-4 shows the picture of the sprectormeter.

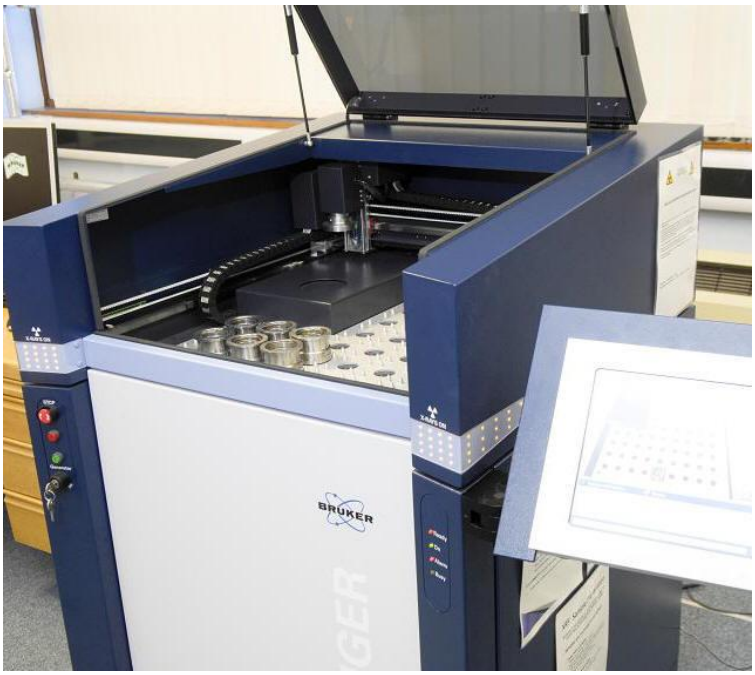

Figure 3-4 Bruker S8 Tiger X-ray Fluorescence spectrometer *(Retrieved from http://chemweb.bham.ac.uk/~hriljaja/MaterialsChemistry/Equipment/Pictures/Bruker_S8.jpg).*

3.2.2.2 N_2 Physisorption

N_2 adsorption/desorption is a common method used for determination of surface area and pore size distribution of solid materials such as ceramics, pigments and catalysts. In this method, the adsorbent is held at a constant temperature, close to the boiling point of the adsorptive. The pressure is increased step by step and held constant for a period of time to allow the adsorption and the equilibrium of the temperature of the adsorbent. The amount adsorbed is measured measuring the pressure change and comparing this to the expected pressure change if the adsorbent were absent. Then, the adsorption isotherm is plotted as amount adsorbed vs. the adsorptive pressure [42]. Surface area is measured by calculating the monolayer coverage and average cross sectional area of N_2

molecule and by making use of the BET theory [43]. Information about pore size and its distribution is retrieved by use of adsorption isotherm and several correlations[42].

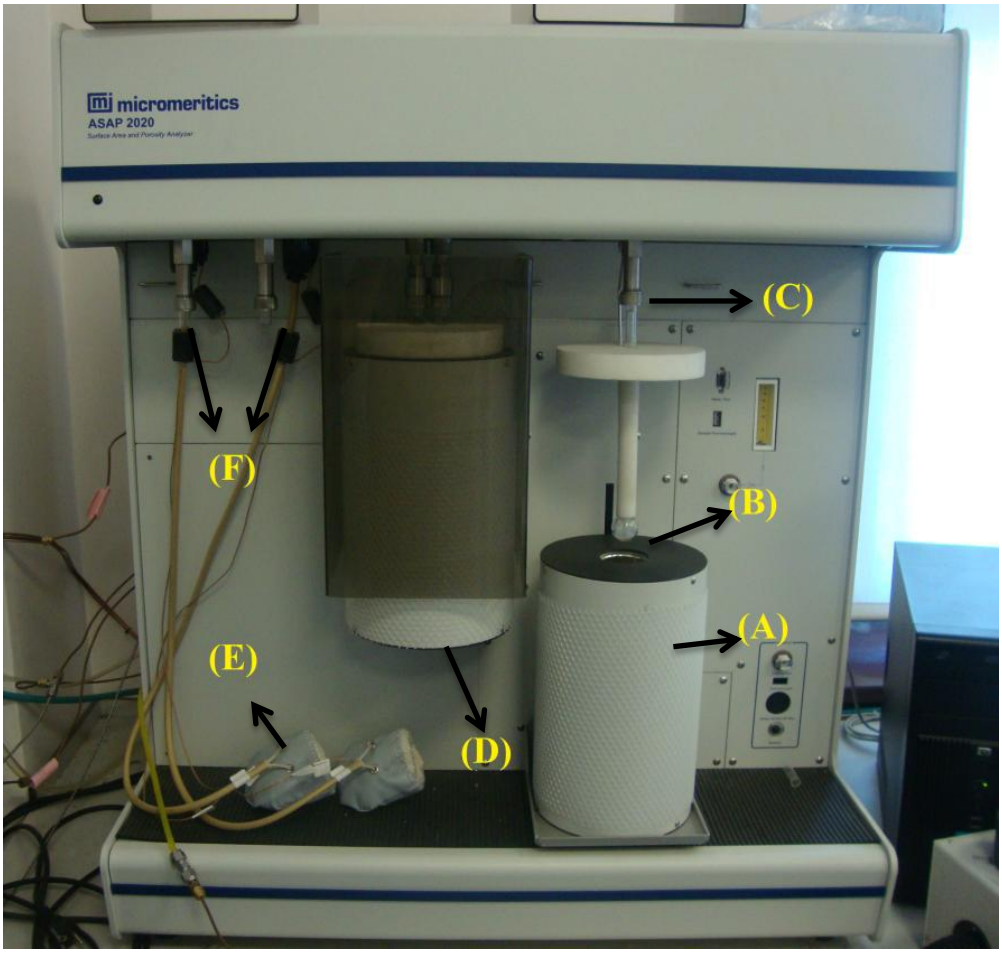

Figure 3-5 Micromeritics ASAP 2020 N2 Adsorption-Desorption Analysis instrument; Analysis dewer (A), sample tube (B), analysis port (C), degas dewer (D), heating jacket (E), and degas ports (F).

N_2 physisorption analysis was performed in Micromeritics ASAP 2020 instrument, see Figure 3-5. First, sample was degassed before analysis. The instrument degas dewer

was filled with liquid N_2 and should be refilled in 3-4 days. Micromeritics' sample tube with glass rod and lid were weighed while it was empty. About 100 mg sample was weighed for the analysis. Crashed sample was filled in the sample tube which was placed degas port 1 or 2 on the instrument. The tube was covered with the instrument heating jacket. Then, sample information was entered from instrument software. Degas conditions were about 300 °C hold temperature and 300 minutes as hold time. Pressure inside the sample tube should drop to a few μm Hg from a few mm Hg. After degas, the sample tube was taken from degas port and weighed. Weight of the empty sample tube was subtracted from weight the sample tube filled with sample and weight of the sample was calculated. Then, the sample tube was covered with a polymeric jacket to keep temperature same throughout the tube. The tube was placed on analysis port. The instrument analysis dewer should be filled up to desired level and checked before each analysis. Weight of the sample was entered to software and analysis was started. 60-point N_2 adsorption/desorption isotherms with a relative pressure (P/P^0) ranging from 10^{-7} to 1 (which required at least 24 h. of continuous operation) were obtained.

3.2.2.3 Temperature Programmed Desorption of NH_3

In this method, after cleaining of the pore surface by using an inert gas, such as He, at elevated temperatures, NH_3 is chemisorbed to the sample. The more the sample is acidic, the higher amount of NH_3 is adsorbed. For instance,pure zeolite in Figure 3-6 has both strong and weak acid sites, which are indicated by two peaks and different temperatures, where as Si-Al/zeolite pellet has a one large peak which corresponds to a moderate acidity. Then, after the removal of physisorbed NH_3 at moderated temperatures , such as 100 °C, desorption of chemisorbed NH_3 is recorded with the help of a detector (thermal conductivity detecor, mass detector etc.) while temperature is increasing with a constant ramp. Later, total acidity of the sample is calculated from the area under the TPD signa vs. Temperature plot and reported as mmol NH_3 adsorbed per gram of sample after the

calibration of the detector. The plot of detector output to the temperature will also yield information about the strong and weak acidic sites since desoprtion of NH_3 would occur at higher temperatures for stronger acid sites.

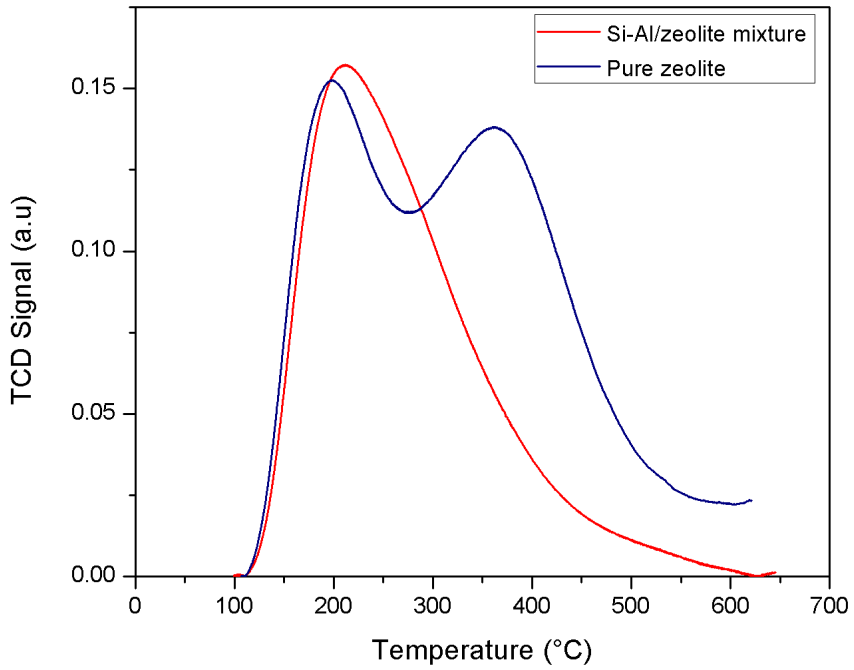

Figure 3-6 Ammonia TPD profiles pellets of Si-Al/zeolite and pure zeolite.

TPD-NH_3 experiments were conducted using a Chemisorb 2750 (Micromeritics) apparatus, see Figure 3-7 . For each experiment about 50 mg of catalyst sample was placed in a U-shaped glass tube and was heated under He flow at a rate of 30 °C min^{-1} up to 500 ^{o}C. Then, the sample was cooled down to 30 °C and treated with NH_3 diluted in helium for 45 min. Finally, the sample was heated to 110 ^{o}C at a rate of 30 °C min^{-1} under He flow to remove the physisorbed NH3. TPD-NH_3 experiments were carried out from 110 to 500 °C with a heating rate of 10 °C/min under He flow.

Figure 3-7 Chemisorb 2750 (Micromeritics) apparatus.

3.2.3 Product Analysis

As later explained in detail at “Experimental Procedures” section, there were two different types of products which were obtained from the runs in which HVGO was used as the liquid feed and from those in which the feed was n-decane. Since n-decane has 10 carbons, hydrocracking reaction products of it are alkanes and iso-alkanes having lower chain lengths and they can be analyzed using a gas chromatography- mass spectrometer

(GC-MS) instrument. On the other hand, HVGO is a mixture of hydrocarbons having a chain length between C21 and C44 [39]. Individual molecules cannot be separated and analyzed using a chromatographic method; thus, standard and simulated distillation methods were used to analyze the products.

3.2.3.1 Gas Chromatography – Mass Spectrometer System

GC is a type a column chromatography in which a gas mixture flows and separates to its components over a stationary phase. Molecules having different affinities towards the stationary phase would leave the column at different times because of the differences in the adsorption strength. Then, outflow of the column is directed to a detector, such as flame ionization detector and mass detector, in order to quantitatively analyze the mixture.

Mass spectrometry is an analytical technique which measures the actual mass of a gas phase sample. First, gas phase is subjected to electron ionization through electron bombardment. In other words, one electron is removed and a + charged molecule which may undergo further fragmentation, producing molecules having lesser mass numbers. The fragmentation pattern is used a fingerprint to identify each molecule. Produced ions are commonly separator by a quadruple ion separator [44]. A detector counts each ion and reports the mass spectrum, which is the relative ion abundance vs. mass to charge ratio plot, see Figure 3-8 for the example of methanol analysis. Summation of all ions passing through the detector yields the total ion chromatogram, which can be used for quantitation purposes.

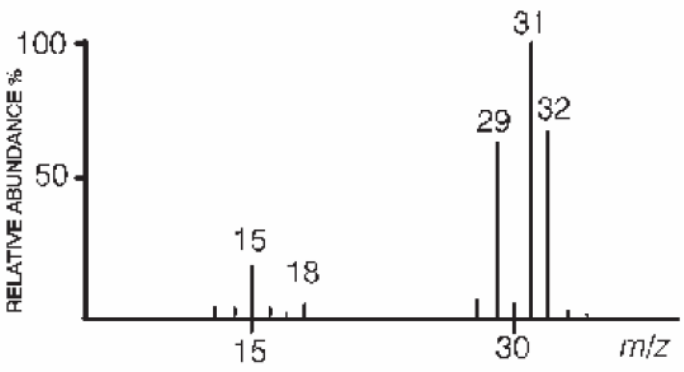

Figure 3-8 Mass Spectrum of Methanol by electron ionization adopted from [44].

The Agilent 6890N GC instrument was used with DB-1 column. Samples were injected to the column with ALS autosampler with an injection volume of 0.5 µl and a split ratio of 1000:1; column flow was set to 0.5 ml/min of mobile gas helium. The oven temperature started from 30 °C and increased to 80 °C with a ramp of 4 °C/min. The Agilent 5975C MSD was used along with the GC. It has a noncoated inert electron ionization source at 150-350 °C. Monolithic hyperbolic quadrupole and triple axis detector were used as ion separator and detector, respectively. shows the picture of GC-MS system.

Figure 3-9 Agilent 6890N - 5975C GC-MS Instrument *(retrieved from http://www.chem-agilent.com/cimg/5975C_7693A-224x90.jpg)*

3.2.3.2 Standard and Simulated Distillation

Liquid products from the HVGO reactions were analyzed by using standard and simulated distillation methods. All distillation experiments were performed by TÜPRAŞ according to the ASTM Standards. Distillation curves, plots of volume or mass recovered versus boiling point temperature, were obtained. ASTM D86 standard was applied to perform the distillation at atmospheric pressure using PAC Optidist instrument. Similarly, distillation at reduced pressures was performed according to ASTM D1160 standard with

the Herzog HDV62 instrument. Since these two methods require higher amount of product (100-200ml), simulated distillation, in which only 1 ml of sample was sufficient for analysis, was chosen to decrease the time required to collect the product. ASTM D2887 standard was followed by using Agilent 6890N GC instrument and SIMDIST software. Figure 3-10 is the distillation curve of HVGO feed used in catalysts testing obtained by ASTM D1160 standard distillation.

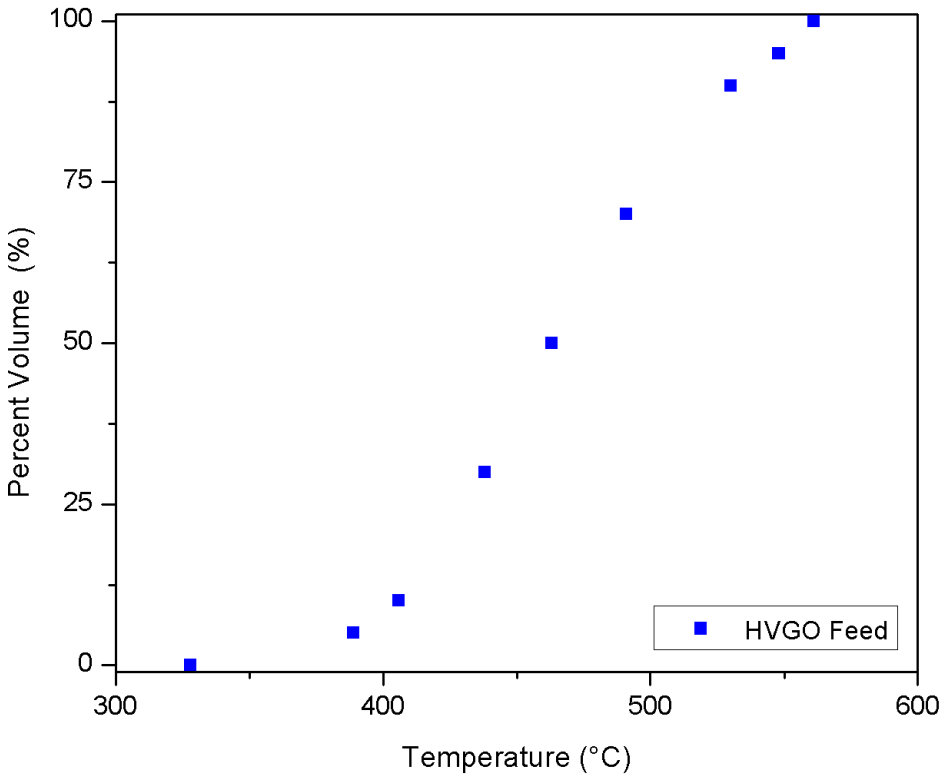

Figure 3-10 Distillation curve of the HVGO feed obtained by ASTM D1160 standard distillation.

3.3 Experimental Procedures

Support and catalyst preparation, material characterization and activity tests of the synthesized catalysts were the main experimental procedures followed in this study. First, each of them is explained in detail at the following sub-sections. Later, the methodology and performed experiments will be presented at the end of this chapter.

3.3.1 Catalysts Preparation Methods

Supported NiO-WO_3 tungsten catalysts were prepared by two different method; incipient wetness impregnation and supercritical deposition. Support pellets from USY zeolite and amorphous SiO_3-Al_2O_3 powders were also prepared before loading hydrogenation metals. Drying and calcination were utilized respectively to bring the catalysts pellets to their final metal oxide forms.

3.3.1.1 Preparation of support pellets

Support materials were prepared by forming extrudates from the powder mixture of USY zeolite and amorphous SiO3-Al2O3 with the use of Ludox HS-40 binder. The experimental procedure was similar to that of [45]. Weighed amounts of powders were mixed in a beaker, after that Ludox binder was added drop wise and the mixture was agitated until a hard paste was formed. From this paste, cylindrical shaped extrudates were formed and cut into 2-3mm pieces. Powders should have a small particle size in order to obtain a smooth paste which can be extruded easily into cylindrical shape. Then, produced pellets were dried overnight at 120 °C to remove the water. Finally, pellets were brought to their final form by calcination at 550 °C (with 20 °C/min heating ramp) for 2 hours under oxygen flow.

Figure 3.11 shows the schematic representation of the procedure. Ludox binder was about 40 to 50 % by weight in the produced supports.

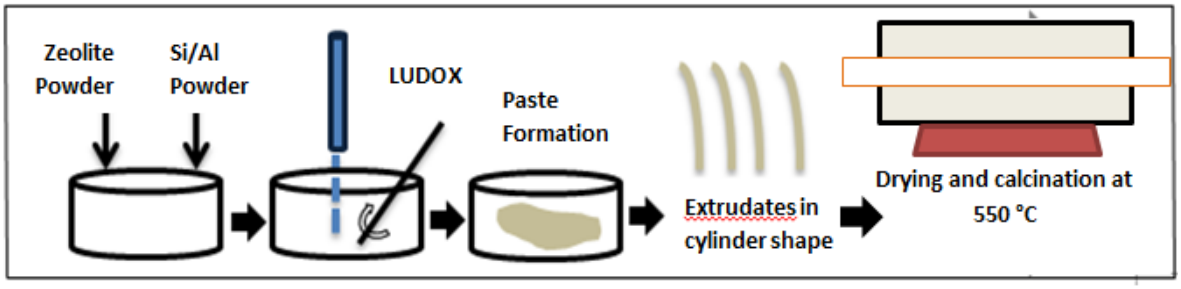

Figure 3-11 Experimental procedure of preparation of support pellets.

3.3.1.2 Incipient Wetness Impregnation

Loading of hydrogenation metals were done by impregnation of aqueous solution of metal salts. Since the volume of the solution is equal to the pore volume of the support, method is called incipient wetness. Desired metal loadings were 24 wt % WO_3 and 6 wt% NiO. First, Nickel nitrate hexahydrate [$Ni(NO_3)_2 \cdot 6H_2O$] and ammonium metatungstate hydrate [$(NH_4)_6H_2W_{12}O_{40} \cdot H_2O$] salts were weighed placed into a beaker and water was added to this mixture. The solution was then stirred quickly and taken into a pipette in order to prevent complex formation. Support pellets were placed on a glass plate and the solution was added drop wise until all the pellets were wet. After 1-2 hour of waiting, pellets were dried overnight (about 14 hours) at 120 °C inside an oven at ambient pressure. Then, the conversion of adsorbed precursors was carried out at ambient pressure under O_2 flow. The impregnated pellets was placed in a custom-made quartz process tube (internal diameter 3 cm, length 57 cm) in a tube furnace (model F1125 Thermolyne) and was exposed to the O_2 at a flow rate of 100 cm^3/min. and heated with a rate of 5 ^oC/min to 550°C and remained at this condition for 4 h. The system was then cooled to room temperature under flowing O_2. Figure 3-11 shows the synthesized materials through the preparation process. Fine yellowish color of the final catalyst indicated the complete

oxidation. Blackish color would have been present in the case of incomplete oxidation of metals.

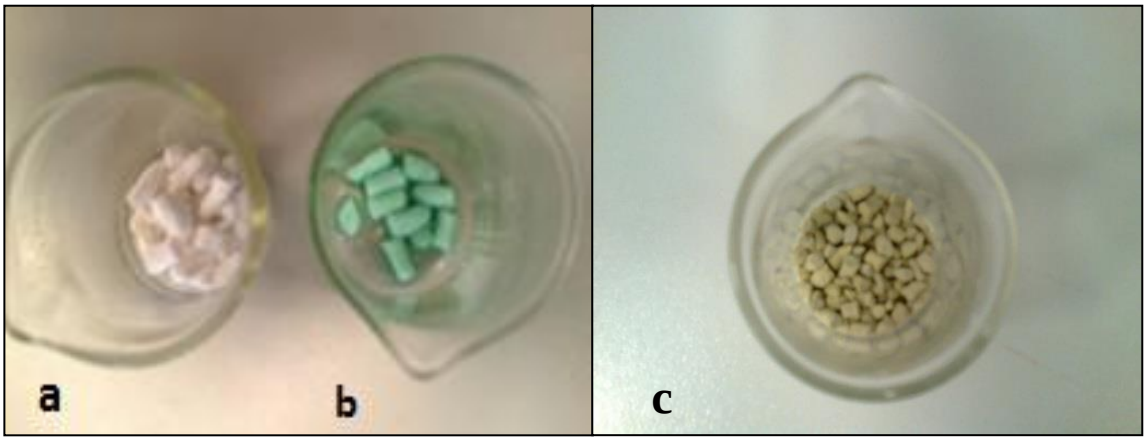

Figure 3-11 Synthesized materials; a) support pellets b) support pellets after impregnation of the metal solution c) final catalyst after calcination.

3.3.1.3 Supercritical Deposition Method

All supercritical deposition experiments were conducted by Dr. Selmi Erim Bozbağ. tungsten hexacarbonyl ($W(CO)_6$) and nickel(II) acetylacetonate ($Ni(acac)_2$) were used as metal precursors.A custom-made stainless steel vessel with a volume of 57 mL was used in SCD experiments. The vessel was equipped with two sapphire windows 2.5 cm in diameter (Sapphire Engineering, Inc., Pocasset; MA), a T-type thermocouple assembly (Omega Engineering), a pressure transducer (Omega Engineering), a vent line, and a rupture disk assembly (Autoclave Engineers) and was sealed with poly(ether ether ketone) O-rings, see Figure 3-12. For each experiment, a certain amount of each of the metal precursors was placed in the vessel along with a stirring bar, and a certain amount of crushed pellet substrate (~2 mm in diameter). A stainless steel screen was placed in the middle of the vessel in order to separate the substrate and the stirring bar. The system was sealed and heated to the desired temperature by a circulating heater/cooler (Cole Parmer, Model

12108-15). The system was pressurized with CO_2 using a syringe pump (ISCO, 260D) up to the desired pressure and kept at these conditions for the desired exposure time. During this process, metal precursors dissolved in $scCO_2$ and adsorbed onto the substrate from the fluid phase. After exposure, the system was depressurized slowly (0.7 MPa/min) using a needle valve (Autoclave Engineers), and the composite sample was removed from the vessel.

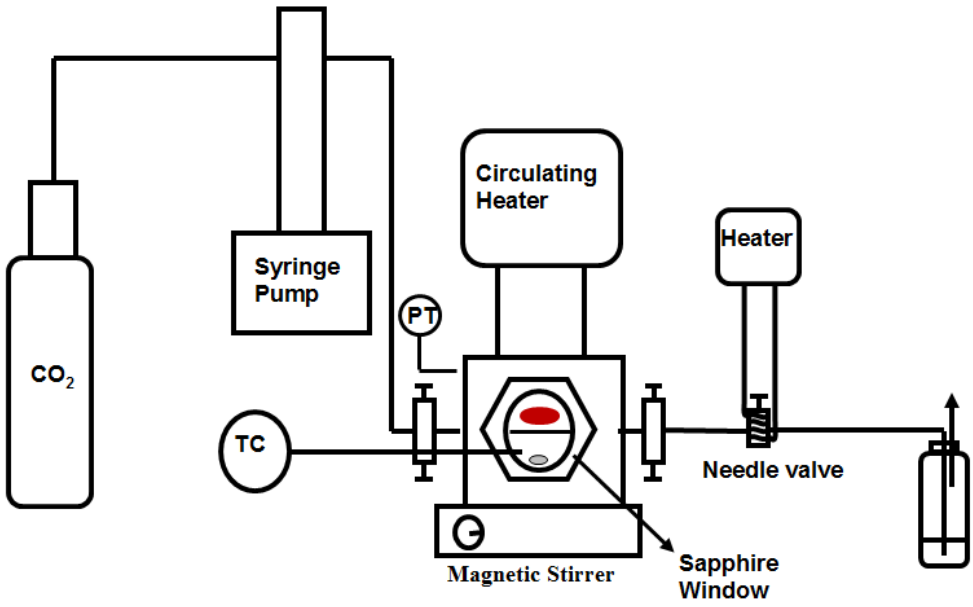

Figure 3-12 Schematic representation of the SCD assembly.

3.3.2 Catalyst Performance Tests

In the catalyst testing experiment, n-decane was used as model feed in preliminary studies whereas HVGO obtained from TUPRAS was used as the real feedstock. Different reactor configurations were assembled to carry out the experiments. Additional heaters, a ZnO bed were placed on the reactor scheme in Figure 3-1 for HVGO runs. MFC's were

calibrated using a soap bubble flow meter before starting experiments. Besides, temperature profile through reactor was obtained by moving the thermocouple inside the thermowell. A uniform temperature profile was obtained in the region where the catalysts would stay. All tests were performed under isothermal and isobaric conditions.

3.3.2.1 Procedure for reactions with n-decane

Performance test were started by loading 10 cc catalysts as in Figure 3-13. Product vessel was filled with approximately 250 ml volume of n-decane. Before pressurizing the reactor and increasing the temperature, a leak test was done using N_2 gas.

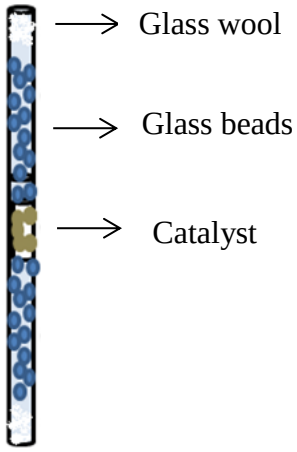

Figure 3-13 Catalyst loading to the tubular reactor.

Once the system was leak free, reactor was filled with hydrogen gas using the by-pass line under the MFC since it would take time to fill the whole volume with 100 sccm gas flow rate. When the reactor pressure reached the operating pressure (100-120 bars), temperature of the reactor furnace was set to operating temperature (380-420 °C). Pre-heater was also set to 80 °C. Gas flow was started with 100 sscm H_2. Decane flow was started with 0.4 ml/min by making the liquid hourly space velocity equal to 2.4 h^{-1} when

the temperature reached the set point value. Temperature of the circulating water in the cooler at the exit of the reactor was set to 15 °C in order to prevent excessive vaporization of light products. After about 1 hour, first liquid products exit from back pressure regulator and started to fill the separator vessel. Then, liquid samples were collected from vessel every one or half an hour and analyzed using GC-MS. Decane flow was stopped when three subsequent analyses yielded the same result by mans of areas under the total ion chromatogram (TIC). Shows the TIC obtained from the test of commercial catalyst. In this graph, peaks at the left side belong to cracking products whereas peaks at the right indicate isomers of n-decane. Moreover, the last peak which emerged at 7.8 min belongs to the feed n-decane, since has the longest n-carbon chain. Finally, all heaters were closed and the reactor was cooled up to 100 °C under hydrogen flow to prevent coking.

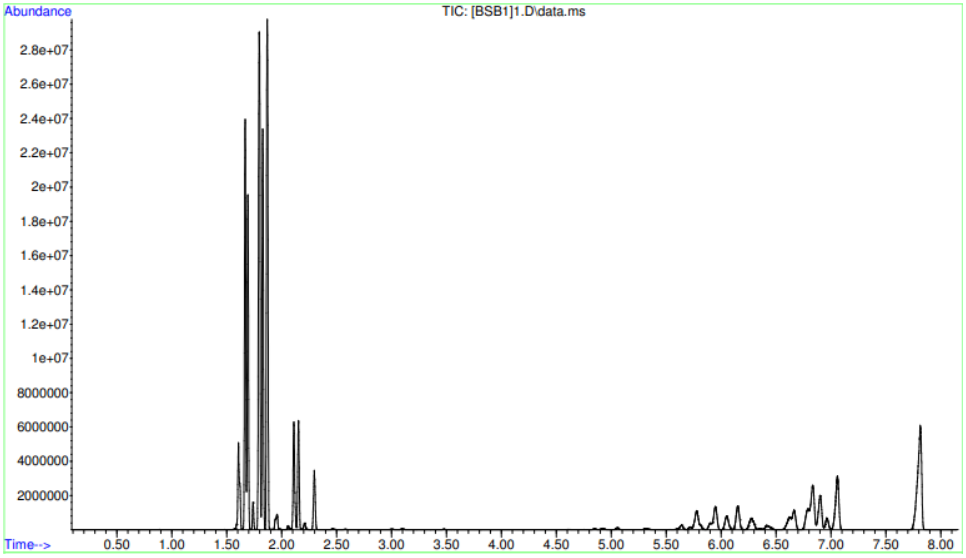

Figure 3-14 Total ion chromatogram of product from the run with commercial catalysts and n-decane feed.

3.3.2.2 Procedure for Reactions with HVGO

The procedure of these tests was same as that of n-decane tests with the exceptions of product recovery and shutdown procedures. Moreover, reactor system was modified the additional heaters and a trapper bed. Since HVGO is at solid state under room conditions, it should be heated up to 60 °C for constant flow through the reactor system. In order to fill the feed vessel, HVGO was heated to 80 °C in an oven. The vessel was also heated to 80 °C by the help of the heating mantle. Then, HVGO was poured quickly to the preheated vessel in order to prevent any solid formation. A heating tape was coiled to the lines between the vessel and HPLC pump, which was kept around 90 °C during the run. Pump head heater was also activated to heat the entrance to 80 °C. Tubing inside the pump was insulated by glass wool in order to prevent any blockage. Preheater after the pump was also used to bring the temperature of the line from pump to reactor inlet to 80 °C. Since H_2S was produced as a hydrogenation reaction product, a ZnO bed having a volume of 10cc was connected to the exit of the reactor. Heat exchanger after the reactor was used to heat the reaction products by setting the circulated water temperature to 80 °C. Lines from this heater exchanger to PBR and separator vessel were heated using a heating fun since they were too long to coil with heating tapes. Figure 3-15 shows the simplified flow diagram of the reactor system after the changes mention above.

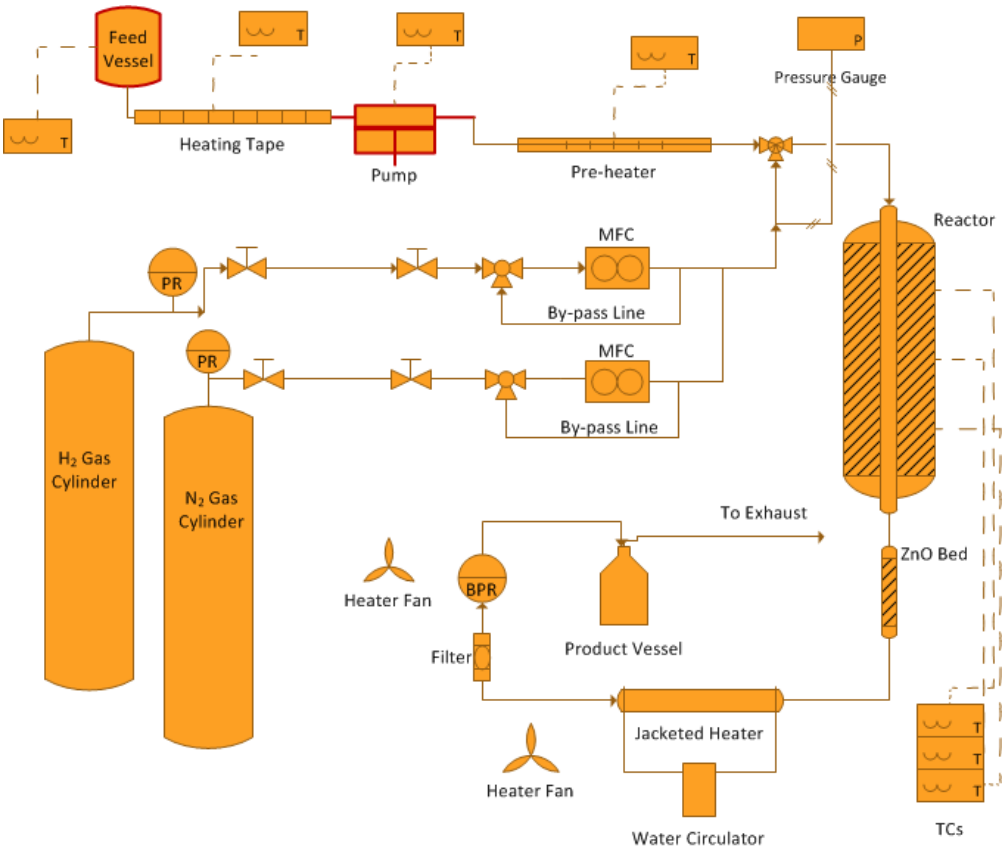

Figure 3-15 Simplified flow diagram of rector system used in the HVGO runs.

Since we could not determine whether the reaction was reached to equilibrium or not by means of GC-MS analysis, about 250 ml of the product were collected after removing the product gathered in first 2 hours. This volume was required for ASTM D1160 distillation analysis. Feed flow could not be shut down immediately after obtaining the required volume of product because HVGO would turn back to in to solid form and block all the tubing lines in the reactor system; thus, a shutdown procedure was used as follows. A three way was placed after the feed vessel. One line from this valve was connected to a tank filled with n-decane. After completion of the run, HPLC pump started to pump n-decane to the reactor by changing the flow way to the n-decane tank with the help of this

valve. Additional heaters were shut down after one hour. N-decane flow was continued with a flow rate of 1-2 ml/min when liquid stream from the exit of the reactor was clean and transparent. In doing so, both tubing lines are catalyst were cleaned from HVGO residues which could lead coking. Finally, all heaters were shut down and reactor was cooled to lower temperatures under hydrogen flow. Experiments were conducted successfully using this procedure. For instance, Figure 3-16 shows the picture of the feed and the product from a run with a commercial catalyst in which the color change indicates the conversion. The liquid product was also stay in liquid form at 35-36 °C.

Figure 3-16 HVGO feed and the reaction product of a sample test with a commercial catalyst.

3.4 Kinetic Modeling of HVGO Hydrocracking

In this study, discrete lumping approach was used in order to make use of distillation curves obtained from experimental data. Lumps were created according to true boiling point values. Aspen HYSYS software was used to create pseudo components for the feed and the product. They were created starting from 2.5 °C with an increment of 10°C to the

final temperature point of the HVGO feed. Mass fractions of the pseudo components were the inputs to the model. Then, mass fractions of the model output were matched with those from the experimental product data in order to estimate the model parameters. Comparisons of rate constant and selectivity were done for different type of catalysts with the help of estimated parameters.

3.4.1 Model for The Hydrocracking Reactor

Since the reactor was running under isothermal conditions, only mass balance was considered for modeling purposes. Moreover, partial pressure of hydrogen was not used in the rate equation since its concentration could be assumed as constant due to the excess use of hydrogen in the performance tests. The system was assumed to have a plug flow, negligible diffusional resistances, and steady-state conditions. It was found that cracking of heavy cuts undergo first order kinetics; thus, the mass balance was constructed for the liquid phase in accordance with this finding [46]. All empiric correlations and model equations were adopted from [47]. The mass balance equation is as follows;

$$M_t \frac{dC_i}{dW} = -k_i C_i + \sum_{j=r}^{N} k_j P_{ij} C_j \qquad i = 1 \; to \; N \qquad \text{Equation 3-1}$$

$$r = i + 2 \; for \; i \geq 13, \quad r = 14 \; for \; i < 13$$

The first term at the right side the equation denotes the disappearance rate of ith pseudo component. Since lumps having boiling points lower than 400 K were assumed not to be cracked, this term $k_i$was calculated as 0 for i < 13. The term with the summation sign indicates the rate of formation of the i^{th} component from higher components. It was assumed that jth component could crack to the ith component when it is equal and higher than (i+2)th component. In the equation above, *M*t is the total mass flow rate of liquid feed to the catalyst bed in kg/h, C_i is the mass fraction of the i^{th} pseudo component, and k_i is the first-order rate constant for cracking of the i^{th} pseudo component in kg-reactant/(kg-catalyst h), N shows the highest pseudo component being cracked, P_{ij} is the probability of formation of the i^{th} pseudo component from the j^{th} pseudo component.

The rate constant of disappearance of a pseudo component was calculated as follows;

$$k_i = K_i k \quad where\ k = \left(\frac{\rho_{HVGO}}{\rho_{catalyst}}\right) A e^{-E/RT}$$ Equation 3-2

In this equation k is an estimated Arrhenius rate constant with values of *A* and *E* as 1.0 x10^7 volume of feed/(volume of catalyst h) and 21 100 kcal/kmol, respectively for hydrocracking of a vacuum gas oil having a boiling range of 573-703 K. The relative rate constant K was calculated according to a polynomial relation with true boiling points, T_b, since rate of cracking increases with the chain length of the hydrocarbon.

$$K_i = D_1 + D_2 T_{b,i} + D_3 {T_{b,i}}^2 + D_4 {T_{b,i}}^3$$ Equation 3-3

Parameters D1-D4 were estimated by the model using experimental data. Some correlations were used to evaluate the product distribution during hydrocracking of each pseudo component [46].The mass fraction of butanes and lighter components generated from hydrocracking of j^{th} pseudo is given as

$$P_{1j} = C \exp[-\omega(1.8T_{bj} - 229.5)]$$ Equation 3-4

Parameters c and ω**,** which are also depends on the catalysts properties, were estimated like D1-D4. Equation 3.5 was used to calculate the yield of all other fractions having boiling points higher than that of butane. where P'_{ij} is the cumulative products yield until the *i*th pseudo component from hydrocracking of the *j*th pseudo component. In the above equation, *yij* is the normalized temperature for the *i*th product formed from the *j*th pseudo component and is given by

$$P'_{ij} = [{y_{ij}}^2 + B({y_{ij}}^3 - {y_{ij}}^2)][1 - P_{1J}]$$ Equation 3-5

where P'_{ij} is the cumulative products yield until the i^{th} pseudo component from hydrocracking of the j^{th} pseudo component. y_{ij} is the normalized temperature for the i^{th} product formed from the j^{th} pseudo component as follows;

$$y_{ij} = \frac{(T_{bi}-2.5)}{[(T_{bj}-20)-2.5]} \quad for\ i = 2\ to\ j-2.\ j = 14\ to\ N \qquad \text{Equation 3-6}$$

Finally, the yield distribution function P_{ij} was evaluated as in the equation 3-7.

$$P_{ij} = P'_{ij} - P'_{i-1j} \qquad \text{Equation 3-7}$$

3.4.2 Solving Method

MATLAB was used to solve model equations.ODE45 solver, which uses the 4^{th} and 5^{th} order Runge-Kutta method, was used to solve ordinary differential equations. Parameters, D1-D4, B, C and $\boldsymbol{\omega}$ were estimated using fminsearch function with an objective function defined as sum of square root of error (difference between weight percentages of pseudo components from model output and experimental data).

Chapter 4

RESULTS AND DISCUSSION

First, preliminary studies using n-decane as the model feed was conducted first. After developing catalysts which had a comparative activity and selectivity to those of commercial catalysts and finding out the necessary operating conditions, heavy vacuum gas oil was replaced with n-decane.

4.1 Catalyst Development and Preliminary Studies with n-decane

4.1.1 Studies with Commercial Catalysts

First experiments with commercial catalysts were performed in order to both understand the reactor system and have reference bases in terms of activity and selectivity. Table 4.1 shows the characterization results of three commercial catalysts in terms of composition, texture and acidity. All three catalysts had the similar weight percentages of NiO and WO_3 as ~6 % and ~25 %, respectively.

Table 4.1 Compositional, textural and acidic properties of commercial catalysts according to XRF, N_2 physisorption and TPD – NH_3.

Catalyst	**CC1**	**CC2**	**CC3**
NiO wt. %	5.91	6.45	5,73
WO_3 wt. %	24.65	28.31	25.76
Pa wt. %	-	0.068	-
BET Surface Area (m^2/g)	221.87	179.05	228.17
Pore Volume (cm^3/g)	0.45	0.37	0.41
Pore Size (nm)	3.38	3.29	2.38
Acidity (mmol NH_3/g)	0.89	0.68	0.81

According to the studies A.M. Alsobaai et al., total acidity of the catalysts enhanced by increasing weight percentages of Ni and W for a USY zeolite support and the optimum values of those are 6% and 23 % by weight, see Figure 4.1 [24].

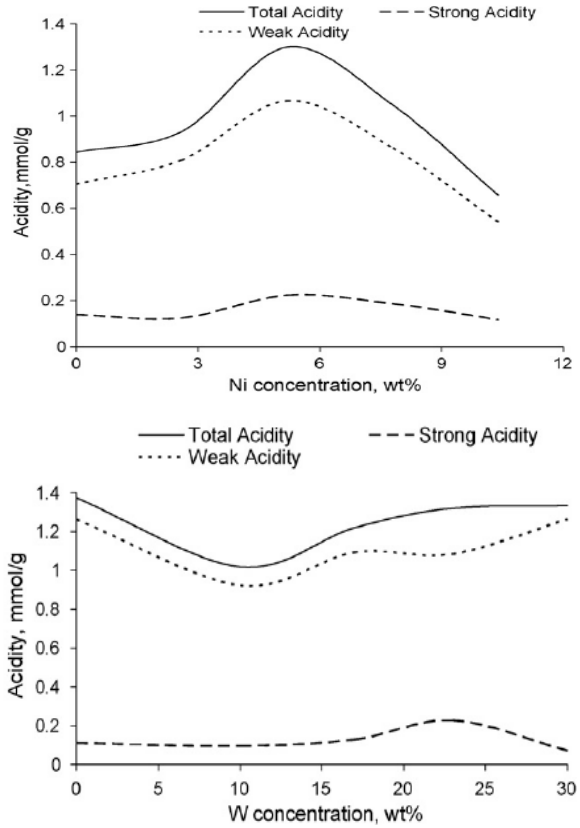

Figure 4.1 The change of acidity of USY supported Ni-W catalysts with the weight percentages of Ni and W, respectively according to the study of A.M. Alsobaai et al. *(adopted from [24])*

Similarly, G.Cui et al. found that optimum total metal loading of NiO-WO_3 was 30 % by weight due to increase in the slab length and stacking degree of W, which enhanced dehydrogenation activity of the catalysts [29]. The study also claimed that excessive loading led to the decrease in the accessible W species, which resulted in decrease in the n-alkane conversion, see Figure 4.2 [29].

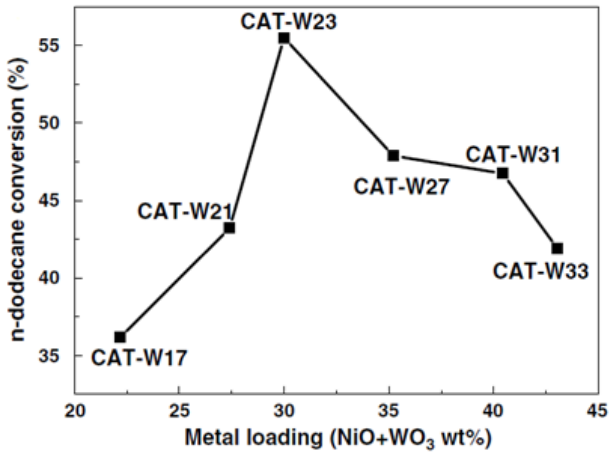

Figure 4.2 Catalytic activity vs total metal loading of catalysts according to the study of G.Cui et al., *(adopted from [29])*

Thus, the metal loading amounts were aimed to 6 % NiO and 24 % WO_3 by weight in the light of both characterization of commercial catalysts and literature [24, 29]. Then, runs with CC2 were performed to find set of operating conditions by which we could compare the testing result of different catalysts. Table 4.2 shows the set of parameters for the initial tests.

Table 4.2 Conditions of performed experiments for Run-1 and Run-2.

Runs	**Run-1**	**Run-2**
Temperature (°C)	300	320
Pressure (bar)	100	100
n-decane flow rate (ml/min)	1	0.2
H_2 flow rate (sccm)	12	24.6
Catalyst amount (cc)	5	10

According to the GC-MS spectra and TIC, almost no cracking and isomerization products were observed from Run-1. The reason was the low amount of catalysts and high value of n-decane /hydrogen ratio. Then, we slightly increased the temperature, decreased the n-decane flow rate while doubling the catalysts amount. From this run, we observed n-pentane, 3-methyl pentane, 3 methyl hexane, n- heptane, 4 methyl heptane, 2 methyl octane being cracking products and 2,6-dimethyl octane, 4 ethyl octane, 4 methyl nonane, 3 methyl nonane being isomers of n-dacane. Note that large amounts of the liquid product were still n-decane. So, we further increased the temperature to increase cracking activity. Similarly, H_2 flow rate increased in order to ensure that we have excess hydrogen.

Table 4.3 Operating conditions for the Run-3 with CC2 and n-decane feed

Run	Run-3
Temperature (°C)	350
Pressure (bar)	100
decane flow (ml/min)	0.1
H_2 flow (ml/min)	61.6
LHSV (1/h)	0.6
H_2/decane (mol/mol)	5
Catalysts amount (cc)	10

In Run-3, appreciable amount of conversion of n –decane was observed according to TIC percent area. Results showed that carbon 6 and decane isomers were the main products of this reaction. It was also important that straight chain products had very less percentage comparing to mono branched products. This means reaction undergoes primary bifunctional transformation [16].

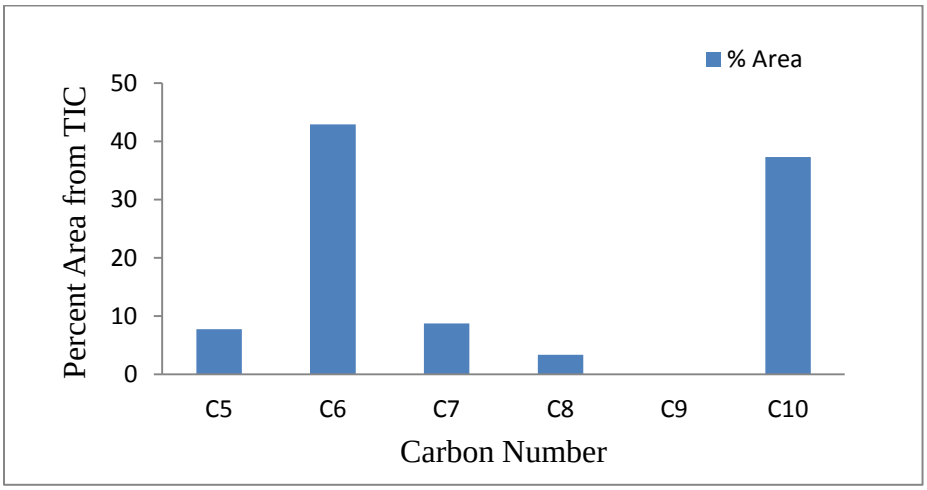

Figure 4.3 Product distribution of the liquid phase for the Run-3 obtained from TIC of GC-MS results.

Figure 4.3 indicates isomerization products have similar percent value with cracking products. Since it was known that isomerization conversion is a unique function of total conversion[16], we decided to increase temperature further to 370 °C, with the change of making LHSV to 2.4 h^{-1}, which was a similar value at the unicracker unit at TÜPRAS by setting the n-decane flow to 0.4 ml/min in order to have primarily cracking products. Since our main aim was to convert vacuum gas oil to diesel fuel via cracking, it was better to have cracking products and high conversion such as 95 %. Moreover, hydrogen flow rate was increased to 101.3 sscm to due to increase in the decane flow rate; so that we had excess hydrogen. Table 4.4 indicates the new set of operating condition according to the changes above.

Table 4.4 Operating conditions for the Run-4 and Run-5 with CC2 with n-decane feed

Runs	**Run-4**	**Run-5**
Catalyst	CC2	CC3
T (°C)	370	370
P (bar)	100	100
n-decane (ml/min)	0.4	0.4
H2 (ml/min)	101.3	101.3
LHSV (1/h)	2.4	2.4
H_2/decane (mol/mol)	2	2

Run-4 and Run-5 resulted in increased conversion and percentage of cracking products, see Figure 4.4. A time stream analysis for Run-4 using GC-MS was conducted to analyze each individual compound, the product distribution and reaction mechanism. Table 4.5 shows the individual compounds and their percent area values.

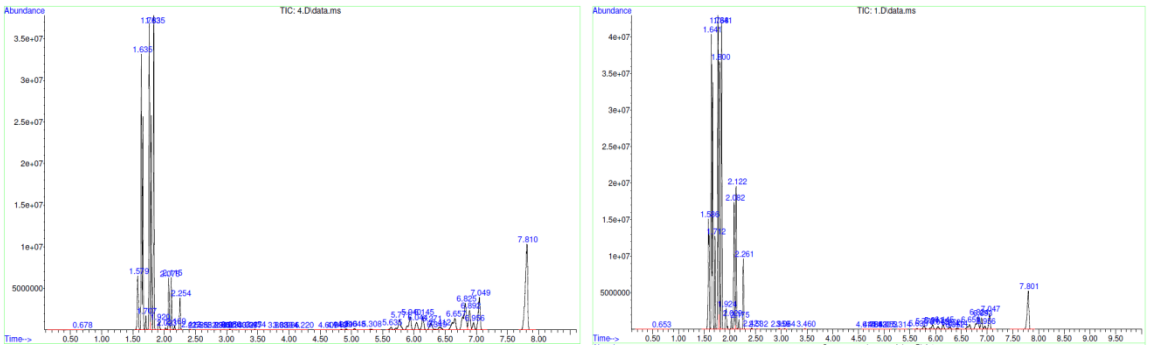

Figure 4.4 TIC from GC-MS for the Run-4 and Run-5, respectively.

Table 4.5 Individual compounds and their percent area values according to TIC from GC-MS results for the Run-4.

Products	%Area - 4 hour	%Area - 5 hour	%Area - 6 hour	%Area - 7 hour	%Area - 8 hour
2-methyl propane	1.62	1.71	1.75	2.00	2.00
butane	1.00	1.10	1.15	1.43	1.30
2-methyl butane	7.82	8.99	9.39	10.40	10.21
pentane	5.56	6.68	7.10	7.81	7.72
2,2-dimethyl butane	0.39	0.50	0.57	0.63	0.65
2 methyl pentane	12.02	13.65	14.60	16.21	16.50
3 methyl pentane	6.56	8.28	9.11	9.83	10.07
hexane	11.12	12.83	13.80	15.15	15.50
2,2-dimethyl pentane	0.49	0.61	0.68	0.72	0.75
3,3-dimethyl pentane	0.09	0.12	0.14	0.14	0.15
2-methyl hexane	2.12	2.56	2.85	2.93	3.01
3-methyl hexane	1.86	2.30	2.59	2.67	2.74
3, ethyl petane	0.16	0.19	0.22	0.23	0.24
heptane	1.27	1.50	1.68	1.73	1.78
2,2,4-trimethyl heptane	0.14	0.14	0.14	0.00	0.00
3,3,5 trimethyl heptane	0.00	0.15	0.15	0.00	0.00
3,5 dimethyl octane	0.86	0.84	0.81	0.71	0.72
2,3,5 trimethyl heptane	0.22	0.22	0.20	0.19	0.18
2,2,3,3 tetra methyl hexane	1.92	1.81	1.74	1.52	1.53
2,5-dimethyl octane	1.94	1.83	1.77	1.56	1.54
5-ethyl,2methyl heptane	1.23	1.17	1.12	0.99	0.98
3,6 dimethyl octane	1.90	1.79	1.69	1.50	1.48
2,6 dimethyl octane	1.22	1.24	1.12	1.00	1.00
2,3 dimethyl octane	0.52	0.56	0.47	0.42	0.41
4,5 dimethyl octane	1.29	1.20	1.10	0.99	1.01
4 ethyl octane	1.66	1.51	1.48	1.26	1.21
5 methyl nonane	1.85	1.68	1.44	1.31	1.34
4 methyl nonane	4.35	3.73	3.57	2.98	2.88

2 methyl nonae	3.13	2.67	2.47	2.10	2.06
3 ethyl octane	0.97	0.88	0.82	0.72	0.72
3 methyl nonane	4.68	4.12	3.81	3.21	3.13
decane	20.02	13.45	10.47	7.66	7.20

also shows that the reaction was reached to steady state after 7 hours from the start of the n-decane feeding. Primary products were mono-branched pentanes, which were 2-methyl and 3 methyl isomers. Besides, both mono and multi branched isomers of n-decane were decreased as the conversion increased Moreover, distribution of the cracked products was found to be independent of the conversion, see **Error! Reference source not found.**.

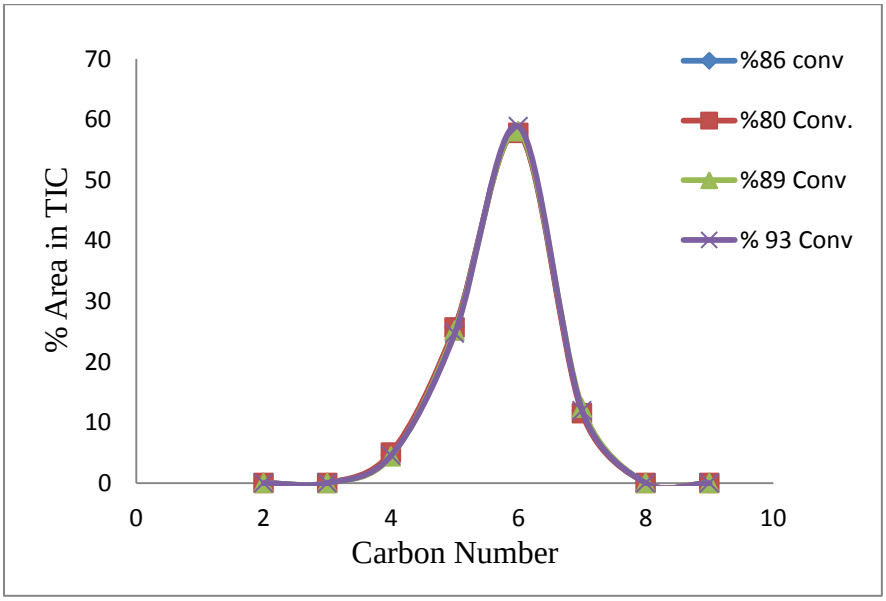

Figure 4.5 Distribution of the cracked products by percent area of TIC from GC-MS data for the Run-4.

Both findings from Figure 4.5 and Table 4.5 were in agreements with the literature and they show that reaction undergoes mostly in primary hydrocracking route [9, 16]. Furthermore, the absence of olefinic and cyclic compounds indicates that the hydrogenation of scission products were successful. Now, we had a good conversion and product distribution with the successful progress of hydrocracking reactions. Thus, operating parameters in Table 4.4 were selected as basis and other performance testing was performed with the same values.

4.1.2 Studies with Synthesized Catalysts

First, a catalysts using amorphous SiO_2-Al_2O_3 pellet was prepared with 24% WO_3 and %6 NiO by weight using incipient wetness impregnation method. Table 4.6 shows the characterization results of the catalyst.

Table 4.5 Compositional and textural properties of Ni/W-SI-01 according to XRF, N_2 physisorption.

Catalyst	**Ni/W-SI-01**
NiO wt. %	6,90
WO_3 wt. %	26,13
Pa wt. %%	-
BET Surface Area (m^2/g)	248,88
Pore Volume (cm^3/g)	0,37
Pore Size (nm)	3,08

Because of the low acidity of the support, 64.9 % area conversion of decane was obtained from the test of this run. Products are mostly isomers of n-decane at the liquid phase and 50.5 % of the converted decane was in the gas phase.

In order to increase cracking activity and acidity of the catalyst supports were prepared with different weight percentages of zeolite and Ludox binder.

Table 4.6 Compositional properties of the supports obtained by gravimetric and XRF measurements

Support Type	**Si/Al-Z-01**	**Si/Al-Z-02**	**Si/Al-Z-03**
Wt fraction of zeolite (Grav.)	0.303	0.563	0.448
Wt fraction of zeolite (XRF)	0.256	0.438	0.389
Wt fraction of Si/Al (Grav.)	0.303	0.070	0.056
Wt fraction of Si/Al (XRF)	0.256	0.055	0.049

Table 4.6 shows the compositions of zeolite and amorphous Si/Al, rest being the SiO_2 matrix from Ludox, of the synthesized supports. Same weight percentages of NiO and WO_3 were loaded to the supports by impregnation method. The final catalysts were labeled as NiW-ZI-01 and NiW-ZI-02 from the supports of the same number. A catalyst labeled as Ni-ZSc-01 was prepared by Dr. Bozbag using the third support by supercritical deposition (SCD). Only 2.1% NiO by weight was loaded to the support since it was his first attempt to synthesized this catalysts.

Table 4.7 Summary of the performance tests with synthesized catalysts for n-decane reactions.

Catalyst name	Support name	% decane conversion w.r.t TIC area	% of decane vol. converted to gas
CC3	-	96.0	72.5
Ni/W-SI-01	Si/Al	64.6	50.5
Ni/W-ZI-01	Si/Al-Z-01	86.9	70.8
Ni/W-ZI-02	Si/Al-Z-02	90.1	81.7
Ni-ZSc-01	Si/Al-Z-03	50.8	39.1
-	**Si/Al-Z-03**	39.7	36.5

Table 4.7 shows the summary of the performance tests for the synthesized catalysts. In all tests, there were almost no olefinic and cyclic compounds and the product distributions were similar. Besides, the introduction of zeolite to the support pellets dramatically increased both normal and cracking activity of the catalysts due the presence of strong acid sides. From the last two entries of the table, we understand that addition NiO to the support increased the conversion by 10 %. Since the hydrocracking mechanism starts with the dehydrogenation, even the small amount of metal loading boosted the conversion. Besides, acid sites from the Ni metal itself might lead to increase in the volume of gas products.

The catalysts Ni/W-ZI-02 seemed to have comparable conversion and selectivity, in terms of percent of the gas products, comparable to the CC3. So this catalyst was selected for the performance tests using the HVGO feed. A micropore BET analysis was conducted for both support and final form of Ni/W-ZI-02.

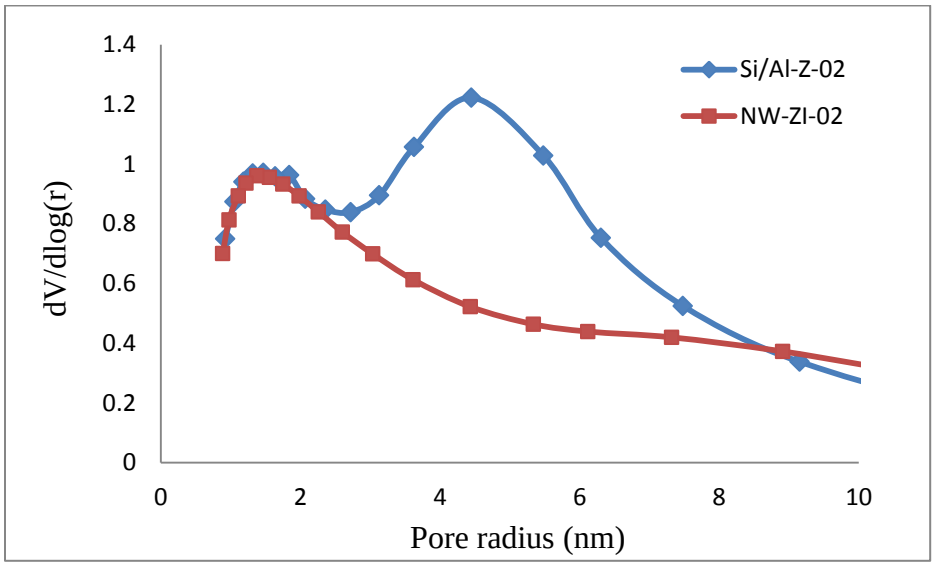

Figure 4.5 Pore size distribution of Si/Al-Z-02 and NiW-ZI-02 samples.

Pore size distributions of the support and catalysts shows that we have micropores coming USY zeolite and mesopores mainly from silica matrix created by binder and Si/Al. Figure 4.1 shows that metal loading decreased the radius of mesopores while micropores remained same. This indicates that metals might be deposited to the mesopores coming from silica matrix instead of micropores of zeolites. Thus, acidic sites were not closed by metal with the loading of the metals. In doing so, the catalyst had a good cracking and hydrogenation activity. The acidity of the catalyst was 1 mmol NH_3/g.

Furthermore, a catalyst using SCD was prepared by Dr. Bozbag by loading the metals to the support prepared by only zeolite powder and binder (by excluding the small amount of Si/Al in Si/Al-Z-02 support). Properties of this catalyst were listed in Table 4.8.

Table 4.8 Compositional, textural and acidic properties of the support and NiW-ZSc-02 according to XRF, N2 physisorption and TPD – NH_3.

	Support	**NiW-ZSc-02**
WO_3 wt.%	-	12.9
NiO wt.%	-	2.2
BET Surface Area (m^2/g)	753.3	311.6
Micropore area (m^2/g)	502.8	202.8
Pore volume (cm^3/g)	0.720	0.325
Average pore radius (nm)	4.89	4.96
Total Acidity (mmol NH_3/g)	0.56	0.77

Performance test of this catalyst resulted in 99.8 % area conversion of decane with 46.9 % of converted decane was in the gas phase. This result was similar to that of the CC1 where the decane conversion was 98.3 % area and 40.6 % of the converted n-decane was in the gas phase. The lower percentage of gas product volume was an indication of middle distillate selectivity by which we can maximize the diesel yield. Moreover, it was found by Dr. Bozbag that some specific groups in USY zeolite involved chemisorption of W and Ni precursor used in synthesis.

If we compare the performances of the catalysts prepared by impregnation and SCD (i.e NiW-ZI-02 and NiW-ZSc-02), we saw that activity of SCD catalyst was higher and it

was also found to be more selective in terms of the percentages of gas products. Moreover, the acidity of SCD catalysts was found to be lower than that of NiW-ZI-02 in contrast to conversion. The reason of this result might be coming from preparation method. In incipient wetness technique, there is a very limited control over the sites on which metal precursors adsorb. The pores are filled with a solution containing metal precursors and subsequently the solvent is evaporated causing the metal precursors to precipitate inside the pores. In reactive SCD however, the metal precursors diffuse in $scCO_2$ within the pores of the support until they reach the specific adsorption site where they chemisorb. Besides, SCD method is known to supply better dispersion of the metals. Moreover, chemisorption of the metals to sites the USY zeolite maight me resulted in better dispersion of the metals. Thus, dehydrogenation activity of the metal might be enhanced due to better dispersion.On th other hand, the acidity increase in the NiW-ZI-02 catalyst was due to acid sites from WO_3 and NiO. In this catalyst, Figure 4.5 shows that we had higher amount of gas products due to cracking of acidic sites of zeolites. So, we can conclude that SCD catalyst had a better performance possibly due to the enhanced dehydrogenation activity. Besides, chemisorption of the metals to USY zeolite sites might also prevented excessive cracking to gas products and so, increase selectivity.

4.2 Performance Testing of Catalyst with HVGO Feed

In this part, we had performed experiments with three different catalysts: NiW-ZI-02 as impregnation catalyst, NiW-ZSc-02 as SCD catalyst and CC1 as a reference catalyst. First, operating condition in Table 4.4 was used to perform a run with CC1, with the exception of an increase of the temperature to 400 °C (since 370 °0C yielded zero conversion). The product was analyzed by D1160 standard distillation. Figure 4.6 shows that low levels of conversion was achieved for this set of operating conditions.

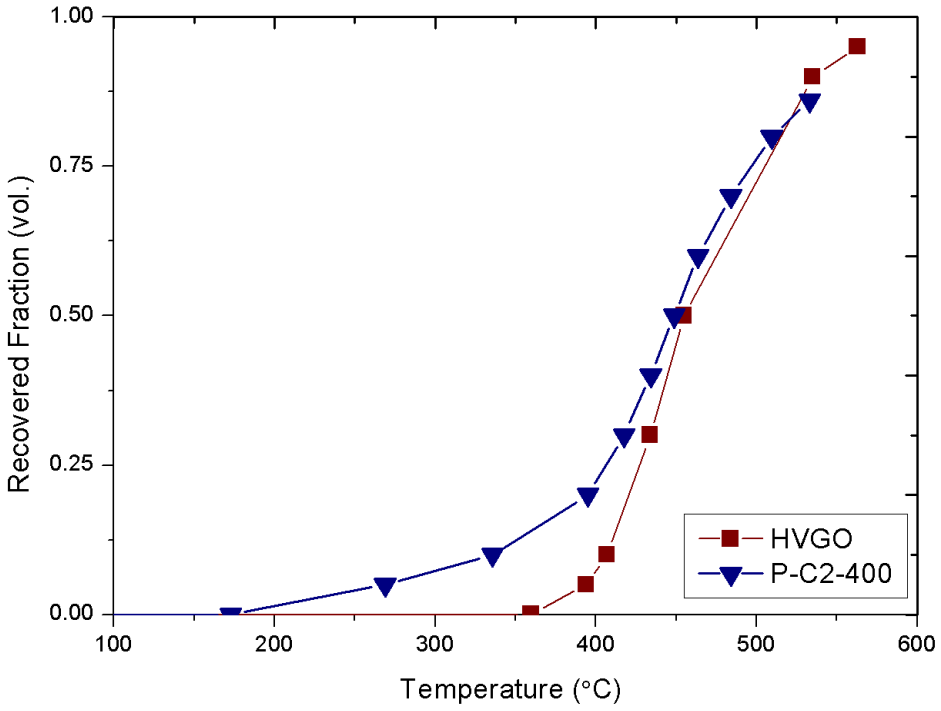

Figure 4.6 Distillation curves for the feed and the product of test with CC2 obtained by ASTM D1160 analysis.

The conversion, selectivity and diesel yield for this part is calculated as follows;

$$\%\ \text{conversion} = \frac{V_{HVGO} - V_R}{V_{HVGO}} \text{ x } 100 \qquad \text{Equation 4-1}$$

$$\text{Diesel yield} = \frac{V_D}{V_{HVGO}} \text{ x } 100 \qquad \text{Equation 4-2}$$

$$S_{diesel} = \frac{V_D}{V_{HVGO} - V_R} \qquad \text{Equation 4-3}$$

$V_{HVGO:}$ Amount of HVGO feed to the reactor
V_R: Amount of unconverted HVGO and heavy cuts
$V_{D:}$ Amount of obtained diesel fraction.
Note that cut point for diesel and kerosene were 230-380 °C and 150-230 °C, respectively.

Initial run with HVGO yielded only 14.1% conversion by volume. So, temperature was further increased to 420 °C and pressure was increased to 120 bar. Then, performance tests of three different catalysts were done at these conditions. Product analysis was performed by ASTM D2887 simulated distillation method. Figure 4.7 and Table 4.9 show the results of the performance test. Distillation curves show that SCD catalysis was superior to impregnation and commercial catalyst. Slight steepness of SCD curve was an indication of selective hydrocracking. The reason of the low diesel yield comparing to CC1 was the low activity of the latter one. Since, the conversion was relatively low for the CC1, most of the products lied in diesel range. Besides, the lowest point of the distillation curves was within the kerosene range, we could conclude that catalysts were performing well in terms of middle distillate selectivity. The slope of the distillation curve of the impregnation catalysts was relatively lower than that SCD. This implies that for typical operational conversion of 95 %, the production of naphtha would be high comparing to SCD catalyst. This result was in agreement with our findings from n-decane tests.

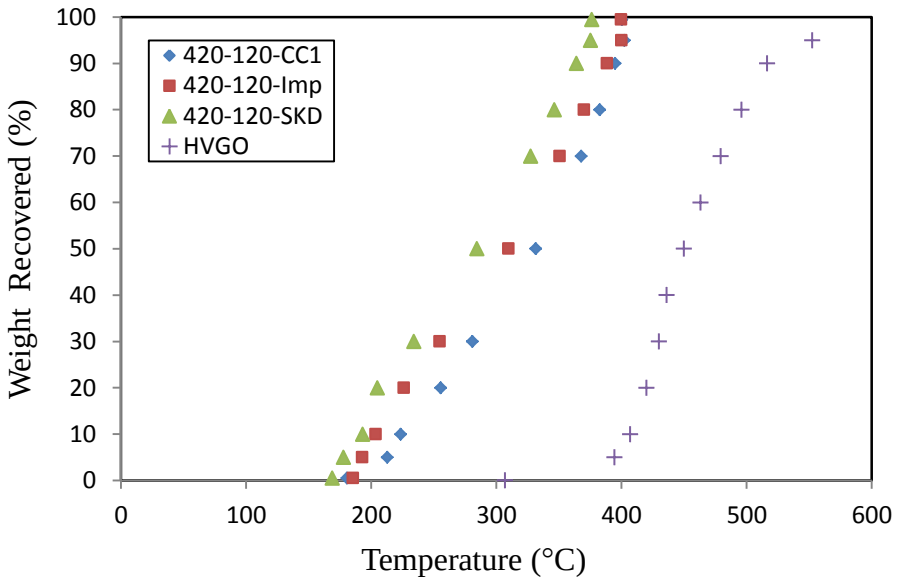

Figure 4.7 Distillation curves for the feed and the products of performance tests performed with three different catalysis obtained by ASTM D2887 analysis.

Table 4.9 Conversion, yield and selectivity values for the catalysts in HVGO studies.

Catalysis	% Conversion	Diesel Yield	Diesel Selectivity
CC1	40.3	28.2	0.70
Impregnation	49.1	27.7	0.56
SCD	60.5	33.8	0.56

4.4 Results of Kinetic Modeling Studies

Kinetic model described in the Chapter 3.4 was used to estimate model parameters for the three catalysts tested in HVGO runs. Below figures show the model fitness to the experimental data for the tested catalysts in terms of distillation curves and weight fractions of pseudo components. Note that HSYS was used to obtain these fractions for products.

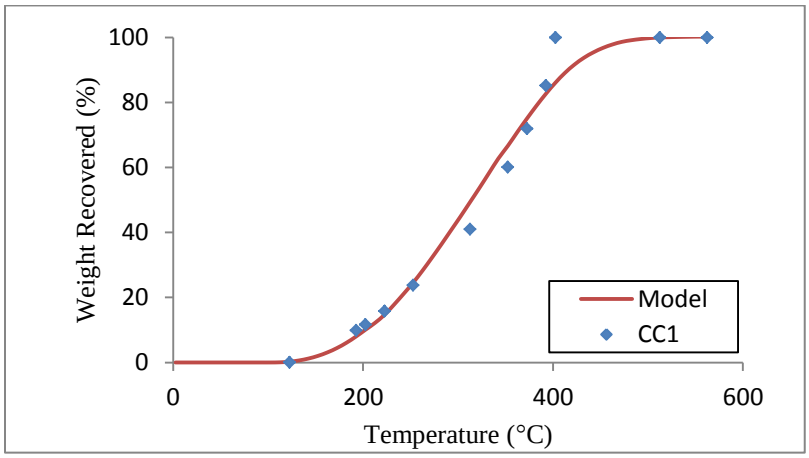

Figure 4.8 Comparison of the distillation curves obtained from the model and experiment for CC1.

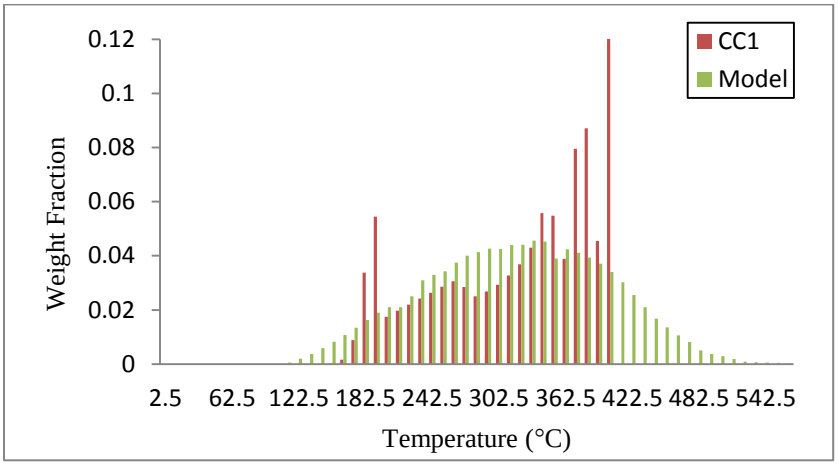

Figure 4.9 Comparison of the weight fraction of the pseudo components obtained from the model and the experiment for CC1.

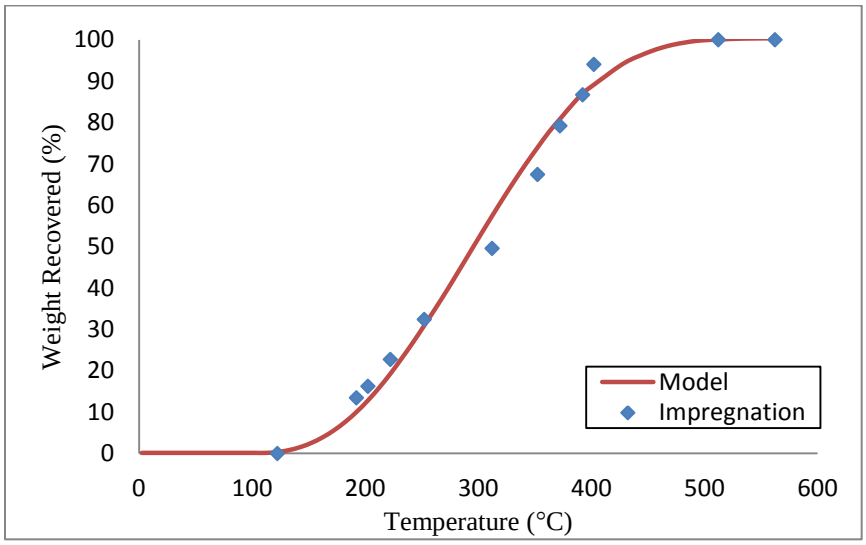

Figure 4.10 Comparison of the distillation curves obtained from the model and the experiment for the impregnation catalyst.

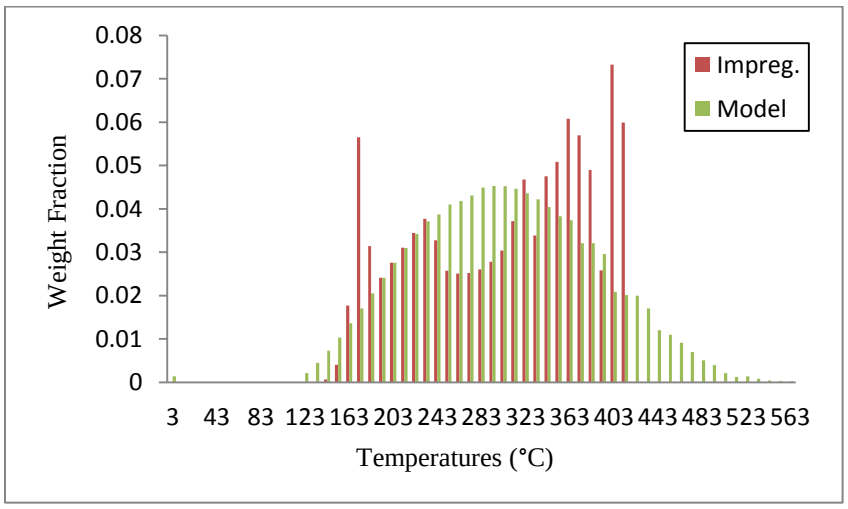

Figure 4.11 Comparison of the weight fraction of the pseudo components obtained from the model and the experiment for the impregnation catalyst.

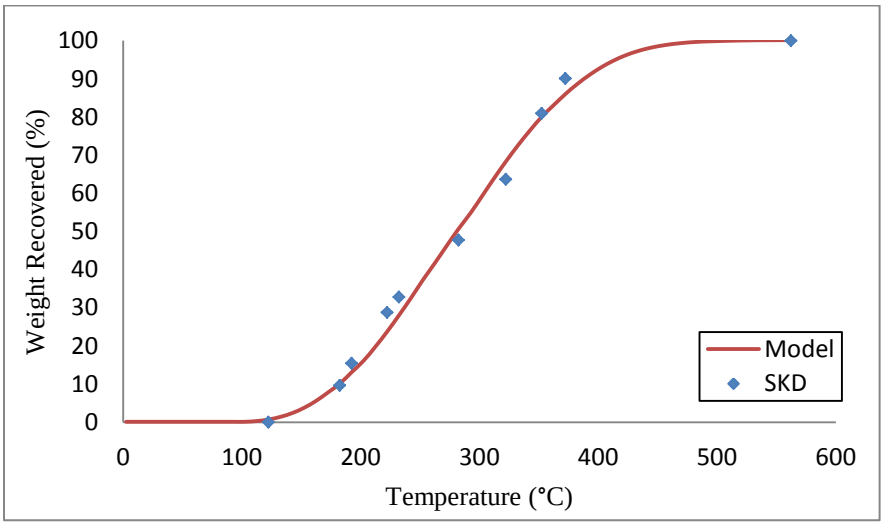

Figure 4.12 Comparison of the distillation curves obtained from the model and the experiment for SCD catalyst.

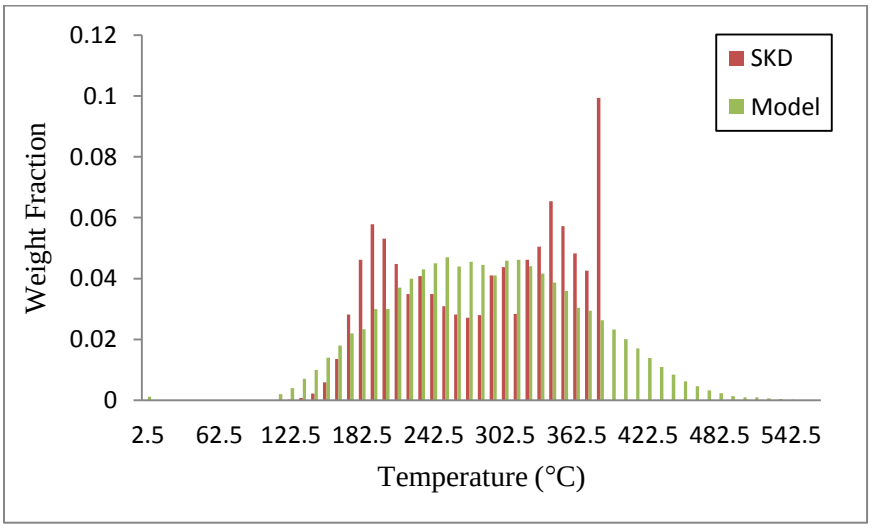

Figure 4.13 Comparison of the weight fraction of the pseudo components obtained from the model and from the experiment for the impregnation catalyst.

Figures 4.9 to 4.14 show that model was working well for the prediction of distillation curves. Prediction of individual lumps was in agreement with the general trend apart from

some very high and low values. Since the objected function was the sum of square root of errors, differences for the individual pseudo components were expectable.

Then, we calculated the disappearance rate of components and draw the plot of k vs. temperature for the heavier cuts which present in HVGO in order to compare the different catalysts.

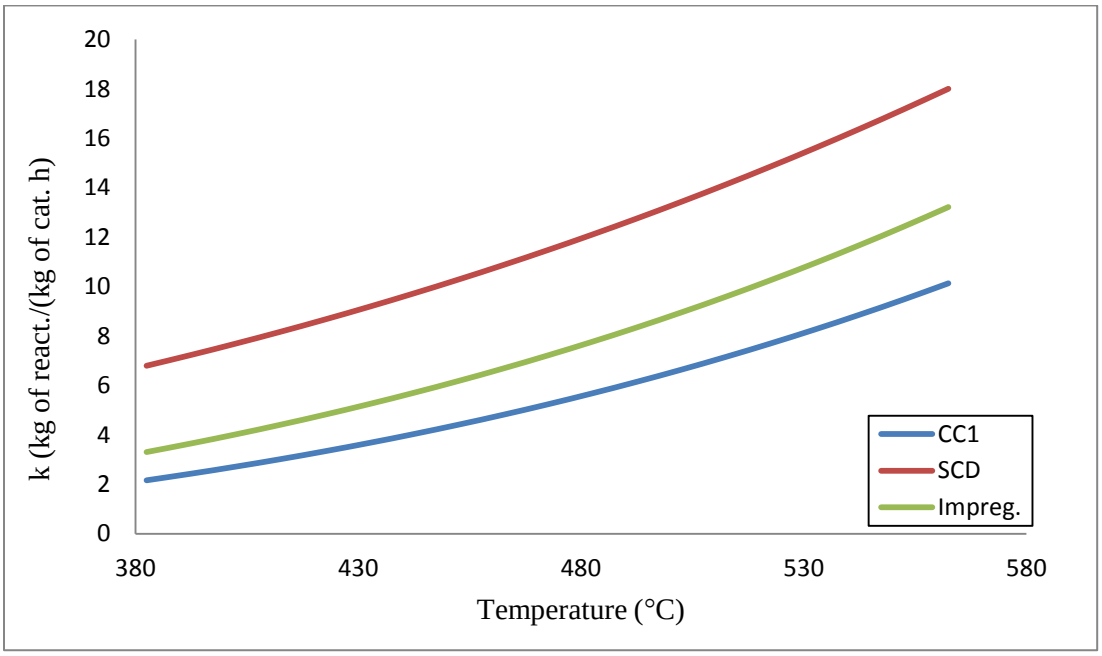

Figure 4.14 Comparison of the rate constant, k as a function of the TBP of the components for different catalysts according to the model results.

Figure 4.14 shows that SCD catalyst had larger rate constants for the heavy cuts than the other catalysts. In order to investigate the selectivity of these cuts to the, we defined kdis, as the rate constant, k, times the fraction of the product between the diesel cut points. The plot of kdis vs. true boiling point of the lumps is as follows;

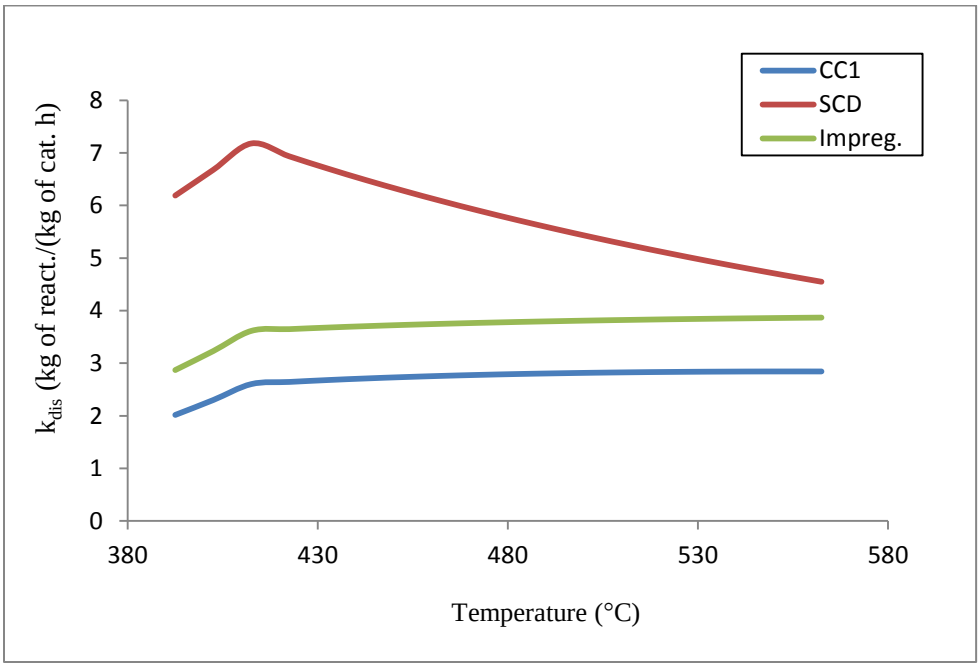

Figure 4.15 Comparison of the diesel rate constant, kdis, as a function of the TBP of the components for different catalysts according to the model results.

Results diesel rate increases up to ~410 °C for all three catalysts. For impregnation and commercial catalysts this value stays relatively constant after this point; however, this value decreases for almost linearly for the SCD catalyst. Moreover, the plot of the diesel selectivity, which is equal to kdis/k, versus temperature was drawn in order to understand the cracking behavior.

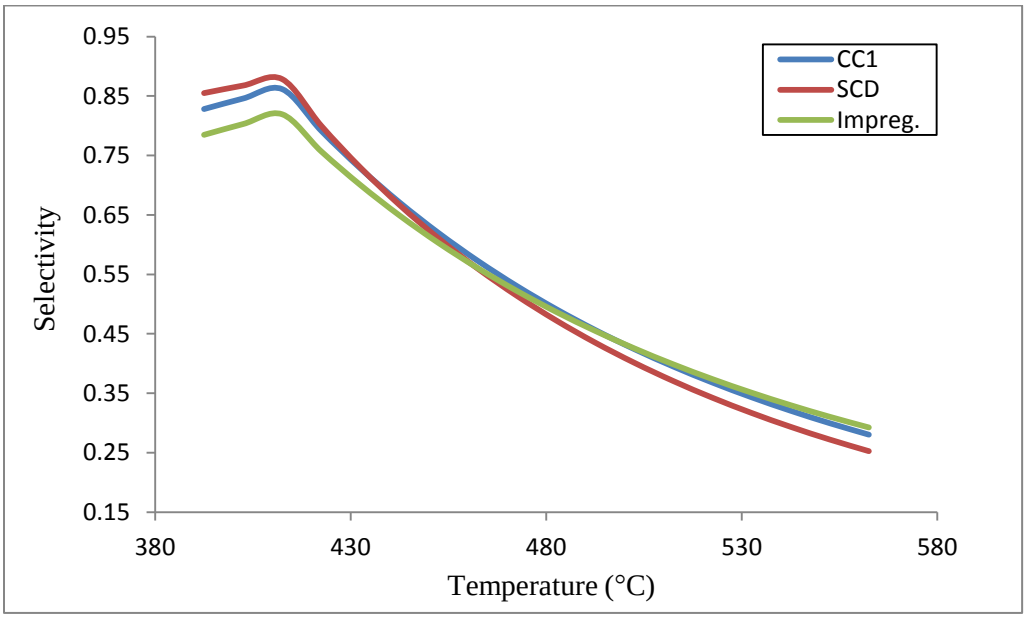

Figure 4.16 Comparison of the diesel selectivity as a function of the TBP of the components for different catalysts according to the model results.

Selectivity values for all catalysts had a similar relation with the temperature. Again, the values increases to the point of 410 °C , this time all of them started to decrease for the heavier cuts. The selectivity of SCD catalysts had higher values for relatively lighter cuts within HVGO. On the other hand, impregnation catalysts had this high selectivity for relatively heavier cuts. This implies that impregnation catalysts performed better for cracking heavier cut whereas SCD catalysts were more selectively crack relative former one. Commercial catalysts had behavior in between those two.

Chapter 5

CONCLUSION

In this study a laboratory scale trickle bed plug flow reactor was developed for processing n-decane and HVGO. Necessary changes in the reactor parts configuration allowed us to pump HVGO and make it flow through the reactor system. N-decane tests results showed that all synthesized final catalysts had a comparable activity and selectivity to the commercial catalysts. The catalyst prepared my incipient wetness was cracking n-decane more to the gas phase compare to the commercial one. BET studies revealed that metal loading was mostly on the mesoporous sites for this catalyst. This led to a high cracking function and increase in the acidity of the support. On the other hand, supercritically deposited catalysts had a higher conversion and selectivity comparing to others. Since some of the metals was chemisorbed the special sites of zeolites, it possibly led to a good dispersion of the metal on the support by creating a balance between acidic and hydrogenation functions. Although, the acidity of the catalyst decreased, better (de)hydrogenation activity and good dispersion boosted the activity and the selectivity of the catalyst. Studies with HVGO also revealed the similar performance results. This time the superior activity of the supercritically deposited catalyst remained same whereas the middle distillate selectivity was only slightly better than other catslyts. Comparison of kinetic parameters via modeling of HVGO also supported this behavior.

BIBLIOGRAPHY

1. Scherzer, J. and A.J. Gruia, *Hydrocracking Science and Technology*. 1996: Taylor & Francis.
2. Speight, J.G., *The Refinery of the Future*. 2010: Elsevier Science.
3. Parkash, S., *Refining Processes Handbook*. 2003: Gulf Professional Pub.
4. Raseev, S., *Thermal and Catalytic Processes in Petroleum Refining*. 2003: Taylor & Francis.
5. *U.S. Refinery Catalytic Hydrocracking Downstream Charge Capacity as of January* U.S Energy Information and Administration.
6. Speight, J.G. and B. Ozum, *Petroleum Refining Processes*. 2001: Taylor & Francis.
7. Gary, J.H., G.E. Handwerk, and M.J. Kaiser, *Petroleum Refining: Technology and Economics, Fifth Edition*. 2007: Taylor & Francis.
8. Company, U.H., *Refining Flow Schem*. UOP Honeywell Company.
9. Weitkamp, J., *Catalytic Hydrocracking-Mechanisms and Versatility of the Process.* ChemCatChem, 2012. **4**(3): p. 292-306.
10. Rezgui, Y. and M. Guemini, *Effect of acidity and metal content on the activity and product selectivity for n-decane hydroisomerization and hydrocracking over nickel–tungsten supported on silica–alumina catalysts.* Applied Catalysis A: General, 2005. **282**(1-2): p. 45-53.
11. Campos, A., et al., *Decane hydroconversion with Al–Zr, Al–Hf, Al–Ce-pillared vermiculites.* Applied Catalysis A: General, 2008. **345**(1): p. 112-118.
12. Jin, H., et al., *Direct synthesis, characterization and catalytic performance of non-sulfided Ni–CsxH3−xPW12O40/SiO2 catalysts for hydrocracking of n-decane.* Fuel, 2013. **112**: p. 134-139.
13. Elangovan, S., *Evaluation of Pt/MCM-41//MgAPO-n composite catalysts for isomerization and hydrocracking of n-decane.* Journal of Catalysis, 2003.
14. Martens, G.G., et al., *A Fundamental Kinetic Model for Hydrocracking of C8 to C12 Alkanes on Pt/US–Y Zeolites.* Journal of Catalysis, 2000. **195**(2): p. 253-267.
15. Jin, H., et al., *Hydrocracking of n-decane over non-sulfided Ni-CsxH3-xPW12O40/Al2O3 catalysts.* Fuel Processing Technology, 2012. **97**: p. 52-59.
16. Steijns, M., et al., *Hydroisomerization and hydrocracking. 2. Product distributions from n-decane and n-dodecane.* Industrial & Engineering Chemistry Product Research and Development, 1981. **20**(4): p. 654-660.
17. Rezgui, Y. and M. Guemini, *Hydroisomerization of n-decane over Ni–Pt–W supported on amorphous silica–alumina catalysts.* Applied Catalysis A: General, 2010. **374**(1-2): p. 31-40.

18. Roussel, M., *Mechanisms of n-decane hydrocracking on a sulfided NiW on silica-alumina catalyst.* Journal of Catalysis, 2003. **218**(2): p. 427-437.
19. Cejka, J., A. Corma, and S. Zones, *Zeolites and Catalysis: Synthesis, Reactions and Applications*. 2010: Wiley.
20. Speight, J.G., *The Chemistry and Technology of Petroleum, Fourth Edition*. 2006: Taylor & Francis.
21. Sato, K., et al., *Role of HY Zeolite Mesopores in Hydrocracking of Heavy Oils.* Journal of Catalysis, 2001. **200**(2): p. 288-297.
22. Maity, S.K. and J. Ancheyta, *Carbon modified Y zeolite used as support material for hydroprocessing catalysts.* Catalysis Today, 2010. **150**(3-4): p. 231-236.
23. Ohshio, N., et al., *Development of zeolite-based catalyst for resid hydrocracking.* Fuel, 2004. **83**(14-15): p. 1895-1898.
24. Alsobaai, A.M., R. Zakaria, and B.H. Hameed, *Gas oil hydrocracking on NiW/USY catalyst: Effect of tungsten and nickel loading.* Chemical Engineering Journal, 2007. **132**(1-3): p. 77-83.
25. Alsobaai, A.M., R. Zakaria, and B.H. Hameed, *Hydrocracking of petroleum gas oil over NiW/MCM-48-USY composite catalyst.* Fuel Processing Technology, 2007. **88**(9): p. 921-928.
26. Burnens, G., et al., *Hydrocracking reaction pathways of 2,6,10,14-tetramethylpentadecane model molecule on bifunctional silica–alumina and ultrastable Y zeolite catalysts.* Journal of Catalysis, 2011. **282**(1): p. 145-154.
27. Cui, Q., et al., *Performance of Zr- and P-modified USY-based catalyst in hydrocracking of vacuum gas oil.* Fuel Processing Technology, 2013. **106**: p. 439-446.
28. Carabineiro, H., et al., *Transient microkinetic modelling of n-heptane catalytic cracking over H-USY zeolite.* Chemical Engineering Science, 2004. **59**(6): p. 1221-1232.
29. Cui, G., et al., *Towards understanding the microstructures and hydrocracking performance of sulfided Ni–W catalysts: Effect of metal loading.* Fuel Processing Technology, 2011. **92**(12): p. 2320-2327.
30. Bozbag, S. and C. Erkey, *Supercritical fluids in fuel cell research and development.* The Journal of Supercritical Fluids, 2012. **62**: p. 1-31.
31. Bozbag, S., et al., *Thermodynamic Control of Metal Loading and Composition of Carbon Aerogel Supported Pt–Cu Alloy Nanoparticles by Supercritical Deposition.* The Journal of Physical Chemistry C, 2013. **117**(13): p. 6777-6787.
32. Yan, P.-h., et al., *Effect of impregnation methods on nickel-tungsten catalysts and its performance on hydrocracking Fischer-Tropsch wax.* Journal of Fuel Chemistry and Technology, 2013. **41**(6): p. 691-697.

33. Francis, J., et al., *Design of improved hydrocracking catalysts by increasing the proximity between acid and metallic sites.* Applied Catalysis A: General, 2011. **409-410**: p. 140-147.
34. Akhmedov, V.M., S.H. Al-Khowaiter, and J.K. Al-Refai, *Hydroconversion of C5–C8 alkanes over Zr-containing supported catalysts prepared by metal vapor method.* Applied Catalysis A: General, 2003. **252**(2): p. 353-361.
35. Liu, J., et al., *A Novel Method of Preparing Ni^|^ndash;Mo^|^ndash;La/^|^gamma;-Alumina Catalysts for Hydrocracking.* Chemistry Letters, 2014. **43**(3): p. 310-312.
36. Hur, Y.G., et al., *Hydrocracking of vacuum residue into lighter fuel oils using nanosheet-structured WS2 catalyst.* Fuel, 2014. **137**: p. 237-244.
37. Alkhaldi, S. and M.M. Husein, *Hydrocracking of Heavy Oil by Means of In Situ Prepared Ultradispersed Nickel Nanocatalyst.* Energy & Fuels, 2014. **28**(1): p. 643-649.
38. Ho, T., *Modeling of Reaction Kinetics for Petroleum Fractions*, in *Practical Advances in Petroleum Processing*, C. Hsu and P. Robinson, Editors. 2006, Springer New York. p. 653-694.
39. Kumar, H. and G.F. Froment, *Mechanistic Kinetic Modeling of the Hydrocracking of Complex Feedstocks, such as Vacuum Gas Oils.* Industrial & Engineering Chemistry Research, 2007. **46**(18): p. 5881-5897.
40. Ancheyta, J., S. Sánchez, and M.A. Rodríguez, *Kinetic modeling of hydrocracking of heavy oil fractions: A review.* Catalysis Today, 2005. **109**(1-4): p. 76-92.
41. Schramm, R., *X-Ray Fluorescence Analysis: Practical and Easy*. 2012.
42. Condon, J.B., *Surface Area and Porosity Determinations By Physisorption*. 2006, Amsterdam, The Netherlands: Elsevier.
43. Brunauer, S., P.H. Emmett, and E. Teller, *Adsorption of Gases in Multimolecular Layers.* Journal of the American Chemical Society, 1938. **60**(2): p. 309-319.
44. E. de Hoffmann, V.S., *Mass Spectrometry - Principles and Applns 3rd ed - E. de Hoffmann, V. Stroobant*. 2007: Wiley.
45. Ali, M.A., T. Tatsumi, and T. Masuda, *Development of heavy oil hydrocracking catalysts using amorphous silica-alumina and zeolites as catalyst supports.* Applied Catalysis A: General, 2002. **233**(1–2): p. 77-90.
46. Stangeland, B.E., *A Kinetic Model for the Prediction of Hydrocracker Yields.* Industrial & Engineering Chemistry Process Design and Development, 1974. **13**(1): p. 71-76.
47. Bhutani, N., A.K. Ray, and G.P. Rangaiah, *Modeling, Simulation, and Multi-objective Optimization of an Industrial Hydrocracking Unit.* Industrial & Engineering Chemistry Research, 2006. **45**(4): p. 1354-1372.

APPENDIX

MATLAB Code for solving model

```
clc;
% clear all;
global D1;  % creating global parameters
global D2;
global D3;
global D4;
global CC;
global B;
global ww;
global k;
global N;
global P;
global Wc

Wc= 5.367e-3;

%parameter = [0.49; 5.2E-3; -2.185E-5; 3.12E-8; 0.35; 0.7; 0.01]; %
inital parameter vector
load('xd');
parameter =x;
D1=parameter(1);   % parameters assigning
D2= parameter(2);
D3= parameter(3);
D4= parameter(4);
CC= parameter(5);
B= parameter(6);
ww= parameter(7);

% data = xlsread(['BoilingPoints.xlsx']); % retrieving raw data from
excell file and transferring to data matrix 58x3
% load('data2.mat');
Tb = data(1:end,1); % assigning true boiling poinÜt lump data
N = size(Tb);
cin= data(1:end,2); % assigning feed mass fraction
creal= data(1:end,3);
kc= (0.8927/2 ) * (1E7)*exp(-21100/(1.987*693)); % this is the equation
for the constant k, values SHOULD be updated.
K = D1 + Tb.*D2 + D3.*Tb.^2 + D4.*Tb.^3 ;
k= K.*kc;
```

```
% for i=1:N
%     if k(i)<0
%         k(i)=0;
%     end
% end
%


for j=14:N   % Yield Function Calculation
    for i=2:j-2
        y(i,j)=(Tb(i)-2.5)/((Tb(j)-20)-2.5);

        P(1,j)= CC*exp(-ww*(1.8*Tb(j)-229.5));
        Pprime(i,j)=(y(i,j)^2+ B*(y(i,j)^3-y(i,j)^2))*(1-P(1,j));

        P(i,j)= Pprime(i,j)-Pprime(i-1,j);

    end

end

% OLD Code here------
[z,cfinal]= ode45('massbalance', [0 Wc], cin) ;


% Pilot Plant Scale Catalysts Weight
%[z,cfinal]= ode45('massbalance', [0 0.300], cin) ;

cfinal(end,:)';
creal;
sum(cfinal(end,:)')

cfinal(end,:)'

Cdeney = data(1:end,10);
Csimul = data(1:end,14);
Cfeed = data(1:end,6);
Cmat=[Cdeney Csimul Cfeed];



createfigure(Tb,Cmat)

for j=1:57
    sum(P(:,j));
```

```
end

for s=34:57
    tdiz =0;
    for m=1: 15
        tdiz= tdiz + P(m,s);
    end
    kdiz(s)=k(s)*tdiz;
end

kdis=kdiz(34:57)'
```

MATLAB Code for mass balance differential equation

```
function dcdz = massbalance(z,C)

global k;
global N;
global P;



dcdz=zeros(57,1);
tot=zeros(57,1);

for i= 1:13  % mass balance
    for j= 14: N
       tot(i) = tot(i)+ k(j)*P(i,j)*C(j);
    end
    dcdz(i)= (-k(i)*C(i)+tot(i))/0.0175; %Experimental
%     dcdz(i)= (-k(i)*C(i)+tot(i))/0.5;  % Pilot Plant Scae
end

tot(56)=0;
tot(57)=0 ;

for i= 14:N  % mass balance
    for j= i+2: N
       tot(i) = tot(i)+ k(j)*P(i,j)*C(j);
       tot(56)=0;
       tot(57)=0 ;

    end
    dcdz(i)= (-k(i)*C(i)+tot(i))/0.0175;
end
```

```
end
```

MATLAB Code for parameter estimation

```
global data
% clear all
% clc

param = [0.5 5E-3 -2E-5 3E-8 2 0.7 0.02]; % inital parameter vector



[x,fval] = fminsearch(@estim,param,optimset('TolFun',1e-
4,'MaxFunEvals',10000000,'MaxIter',159))


save('xd.mat','x');


function errf = estim(parameter)


global D1;  % creating global parameters
global D2;
global D3;
global D4;
global CC;
global B;
global ww;
global k;
global N;
global P;
global data
global Wc

Wc= 5.367e-3;

D1=parameter(1);   % parameters assigning
D2= parameter(2);
D3= parameter(3);
```

```
D4= parameter(4);
CC= parameter(5);
B= parameter(6);
ww= parameter(7);



Tb = data(1:end,1); % assigning true boiling point lump data
N = size(Tb);
cin= data(1:end,2); % assigning feed mass fraction
creal= data(1:end,3);
kc= (0.8927/2 ) * (1E7)*exp(-21100/(1.987*693)); % this is the equation
for the constant k, values SHOULD be updated.
K = D1 + Tb.*D2 + D3.*Tb.^2 + D4.*Tb.^3 ;
k= K.*kc;

% for i=1:N
%     if k(i)<0
%         k(i)=0;
%     end
% end
%

for j=14:N   % Yield Function Calculation
    for i=2:j-2
        y(i,j)=(Tb(i)-2.5)/((Tb(j)-20)-2.5);

        P(1,j)= CC*exp(-ww*(1.8*Tb(j)-229.5));
        Pprime(i,j)=(y(i,j)^2+ B*(y(i,j)^3-y(i,j)^2))*(1-P(1,j));

        P(i,j)= Pprime(i,j)-Pprime(i-1,j);

    end

end

% OLD Code here------
[z,cfinal]= ode45('massbalance', [0 Wc], cin) ;%OPTIONS);

for i=1:N
    err(i)=100*sqrt((cfinal(end,i)-creal(i))^2);  % TRUE

end
```

```
errf=sum(err)

end
```

USY Zeolite (331HSA) Specifications

Cation type: H^+

SiO_2/Al_2O_3 (mol/mol) = 6

Acidity via NH_3-TPD (mmol/g) = 2

Surface Area (BET, m^2/g) = 650

Crystal Size (µm) = 0.7-1

Silica Alumina Specifications

Mesoporous, surface area 230 m^2/g

Amorphous

Negligible acidity (as compared to zeolite)

1,50 mm trilop, 448 m^2/g surface area, 0,72 cm^3/g pore volume, 93 Å pore diameter

Model parameter values

	D1	D2	D3	D4	c	b	w
SCD	0.178	0.0047	9.52E-06	6.26E-08	-0.717	1.696	0.036
CC	-3.21	0.0204	-6.48E-05	1.26E-07	-11.87	1.461	0.075
Impregnation	-2.66	0.0159	-4.92E-05	1.27E-07	-8.961	1.170	0.094

Temperature Profile along Reactor

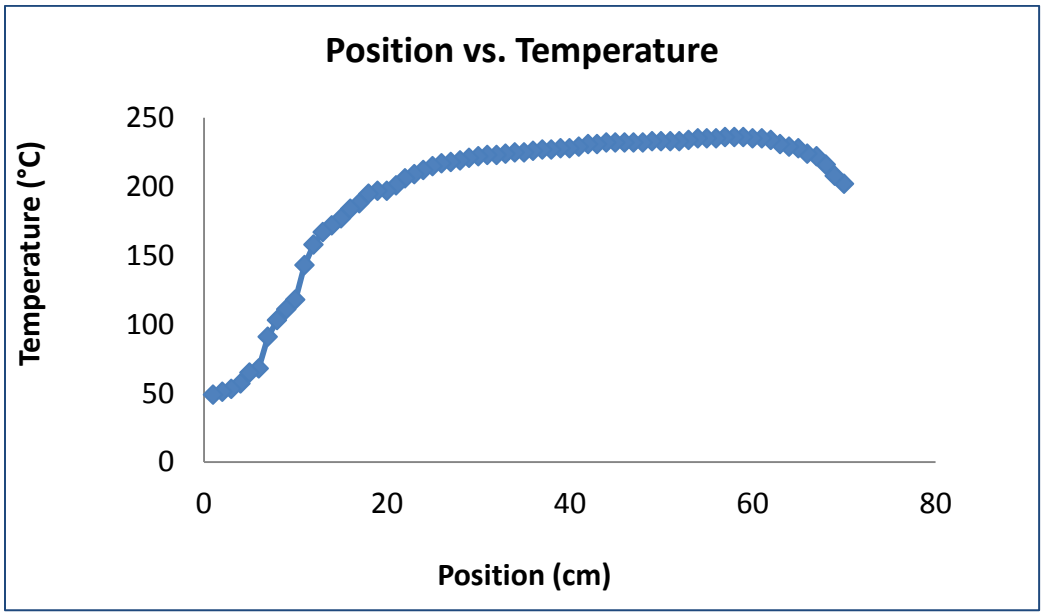

Calibration of MFC for Hydrogen